Seismic and Atmospheric Measurement Utility Stations (SAMUS)

Final Project Report

for

AE 4342 – Space System Design

Daniel Guggenheim School of Aerospace Engineering
Georgia Institute of Technology Spring 2022

21 April 2022

Anthony Limiero, Ethan Hembree, Garrett Drieband, George Frampton, Harrison Stewart, John Ryu, Thomas Baker, Dominic Hernandez, Gabi Nwachukwu

SAMUS Mission Fact Sheet

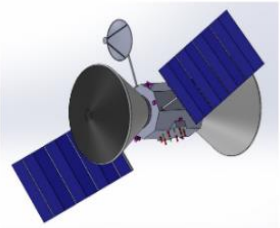

Mission Team

Principal Investigator (PI) - Dominic Hernandez
Deputy Principle Investigator (DPI) - George Frampton

Antthony Limiero
Ethan Hembree
Garrett Drieband
Harrison Stewart
John Ryu
Thomas Baker
Gabi Nwachukwu

Mission Overview

The Science and Atmospheric Measurement Utility Stations (SAMUS) will launch on the 30th of October 2026 aboard a heavy class launch vehicle bound for Mars. After being put on an interplanetary transfer orbit, it will arrive at Mars on August 20th, 2027. After spending 19 weeks aerobraking in Mars' atmosphere, the spacecraft will perform a circularization burn to enter a 3500 km altitude orbit. From this orbit, it will release two landers which each perform a deorbit burn to land on the Martian surface.

Science Goals and Objectives

- Understand the origin and evolution of Mars as a geological system
  - Determine whether seismic activity is a result of tectonic activity
  - Determine the size and characteristics of the Martian core
- Understand the processes and history of climate on Mars

Payload and Instrumentation

- **Seismic Experiment for Interior Structure (SEIS)** will provide data for producing a model of the Martian interior around the Valles Marineris. By detecting and analyzing R3 seismic waves, the experiment will verify if Martian seismic activity is a result of tectonic activity. In addition, it will ascertain information regarding the size and makeup of Mars' core.
- **Rover Environmental Monitoring Station (REMS)** will help the mission assist the ESA-NASA Trace Gas Orbiter in collecting Mars atmospheric data for understanding the climate history of Mars. By collecting temperature, pressure, wind speed, and UV radiation data, REMS will provide the auxiliary environmental telemetry for Mars climate modeling.

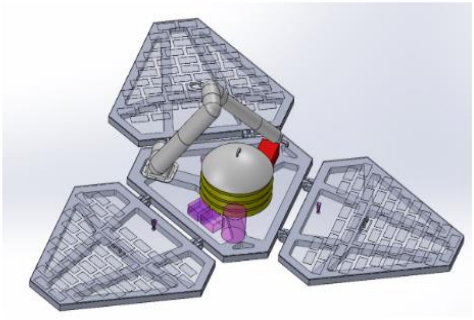

Seismic and Atmospheric Measurement Utility Stations (SAMUS)

Milestones

Phase A Start Date:
June 1st, 2022

Launch Date:
October 30th, 2026

Mars Arrival Date:
August 20th, 2027

Key Metrics

$465,151,071.82 Projected Mission Cost

2-3 Years Expected Mission Lifetime

3,972.23 kg Spacecraft Launch Mass

23.6% Mission Mass Margin

2 Science Instruments

Mass Breakdown

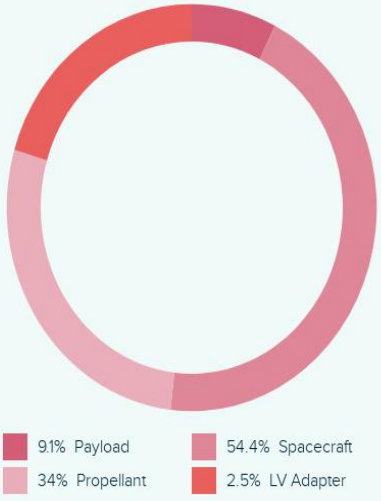

Table of Contents

Science Investigation

The Martian geologic process is unique with respect to solar system exploration because it possesses similarities to Earth throughout Earth's lifetime. It is believed that Mars previously had a magnetic field produced by a molten core, and experienced plate tectonics – just as Earth does today. Currently, the magnetic field surrounding Mars is extremely weak, and all tectonic activity is thought to have ceased. As stated in the 2013-2022 NASA Planetary Science Decadal Survey, and MEPAG goal III, NASA aims to model the interior structure of Mars and understand how core separation and interior processes are related to the initiation and cessation of tectonic processes. This decadal survey also outlines NASA's intent to understand how these interior events occurred and how the magnetic field and structure of the planet were affected as a result. NASA deems the creation of a geophysical data collection network necessary to answering the previously stated science questions, and ultimately achieving the goal of understanding the origin and evolution of Mars as a geological system. Seismic data can be used to infer information of the Martian interior structure, such as: lithosphere/crust structure and thickness, current seismic and volcanic activity, depth of crust magnetization, and the structure of surface highs and lows.

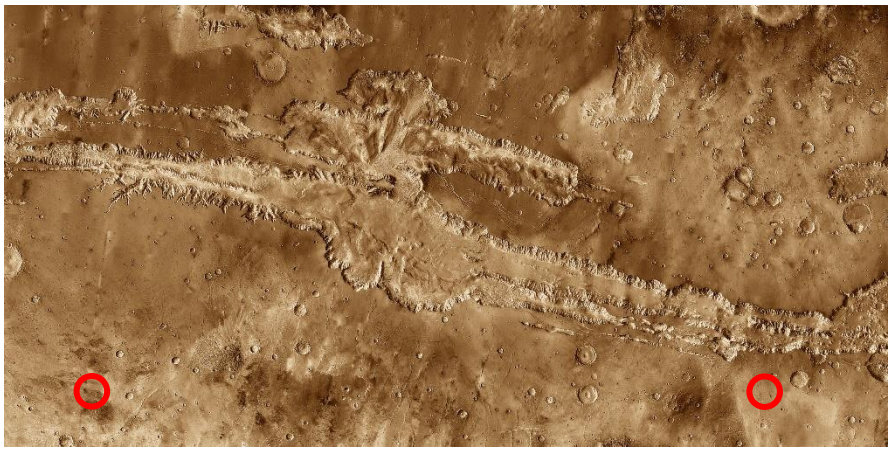

Figure 1 Mosaic image of Valles Marineris captured by NASA's Mars Odyssey orbiter, overlayed with planned SAMUS landing sites.

The primary science goal of the SAMUS mission is to further understand of the origin and evolution of Mars as a geological system. The use of seismometers to detect seismic waves has been integral to our modeling and understanding of the internal structure of Earth, and the same methodology can be applied to Mars [11]. In order to further understanding of the Martian interior in the same manner, our objective is to deploy a small network of seismographs to the Martian surface. This pair of seismographs will be located at either end of Valles Marineris, as seen in Figure 1, a 3,000 kilometer by 600-kilometer valley whose origins are still unknown. Currently, the only functional seismograph on Mars is on board the Mars InSight lander. The Mars InSight lander recently detected a magnitude 4.2 quake of origin that has not been accurately located. One possible point of origin is Valles Marineris [3]. It is also estimated that lava may have flowed in Valles Marineris within the last few million years [3]. The possibility of recent geological activity makes this landing site one of great scientific interest. A single 3-axis seismograph is capable of roughly locating the origin of seismic events, however multiple are required to obtain an accurate epicenter. Sending two 3-axis seismographs will allow for the location of seismic events with much more accuracy, and modeling of the internal structure of Mars. However, the location and analysis of seismic events should not be limited to the area surrounding Valles Marineris. The seismographs being sent to Mars will be capable of individually locating and collecting data on seismic events originating anywhere within the planet. This instrument performance and landing site location allow for seismic information to be collected on the planet as a whole, while enabling higher quality epicenter locating at a location of seismic interest. The seismic information collected will be used to fulfill three top level mission requirements pertaining to seismic data collection. This mission will enable the detection of seismic epicenters to within 100 kilometers globally. This mission will positively determine whether recent seismic activity local to Valles Marineris is due to tectonic activity. And finally, this mission will determine the radius of the Martian core to ± 250 kilometers. These requirements will fulfill the outlined science objective and make progress towards achieving the goal of understanding the origin and evolution of Mars as a geological system.

What can vibrations in the ground tell us about the Martian interior? Seismic events within the Martian crust will create seismic waves that propagate through Mars with different characteristics depending on the composition

and structure of the planet. These waves can be divided into two categories, body waves and surface waves. As each name implies, body waves travel through the body of the planet while surface waves travel along the surface of the planet. Surface waves will be primarily used to locate any seismic event. Surface waves can be broken down into three categories of waves, R1, R2, and R3 waves, where R is short for Rayleigh. An R1 wave is a surface wave that has traveled across the planet's surface from the epicenter of a seismic event to the seismograph along the shortest path. R2 waves are waves that have traveled across the planet's surface from the epicenter directly to the seismograph along the longest path. An R3 wave is a wave previously detected by the seismograph that has traveled, along the surface, around the planet and been detected again. If three or more seismographs are used, the time of measurement of R1 surface waves at each seismograph can be compared to triangulate the location of the epicenter with accuracy dependent on the material model of the surface of mars –which will continually increase as more information of the Martian surface is collected. However, seismic activity can still be located, with less accuracy, using a single seismograph. In order to locate an epicenter with a single seismograph three key measurements must be made. The seismograph must be capable of, measuring the direction of oncoming surface waves, detecting R1 waves, and detecting R2 waves. For this mission, requiring the ability to measure wave direction and R3 of seismic events will ensure these requirements are met. These capabilities require seismic measurements to be made along two axes, however with a third axis body waves can be measured as well. Body waves can further be divided into two categories: P-waves and S-waves. P-waves, or primary waves, are pressure waves that are transmitted through the compression and expansion of the crust parallel to the direction of propagation –these waves are the first to reach a seismograph after a seismic event. An S-wave, or secondary wave, propagates slower than P-waves and travel with motion perpendicular to the direction of propagation –think shaking a rope up and down rapidly. P-waves are able to travel through solid, liquid, and gaseous substances, while S-waves are only able to travel through solid substances. Primary and secondary waves also travel with characteristics dependent on the substance they are traveling through. The speed at with P-waves and S-waves travel are dependent on the density of the material in which they are traveling. As a result, refraction of seismic waves is observed when a wave passes from one material to another material with different properties. The differences in propagation between different types of waves and dissimilar materials allow for inferences of the internal Martian structure and composition to be made. For example, if the location of an epicenter is found via surface wave measurements, the measurement (or lack thereof) of P-waves and/or S-waves can allow the size and makeup of the planet core to be inferred. S-waves will not travel through a liquid outer core, thus creating a shadow where no S-waves can be measured. A similar P-wave shadow may be experienced, as P-waves will be refracted when entering a liquid layer, or solid layer of different density, and may not reach a portion of the planetary surface. Figure 2 illustrates these phenomena. If enough seismic events are located and detected, the size of the molten and solid portion of the Martian core can be measured. Similarly, differences in wave propagation through the crust of Mars compared to the Martian mantle can be used to determine the thickness of the crust. Because the discovery of the primary and secondary wave shadows is dependent on the location of the seismograph relative to the epicenter, it is advantageous to have instruments located throughout the surface of the planet.

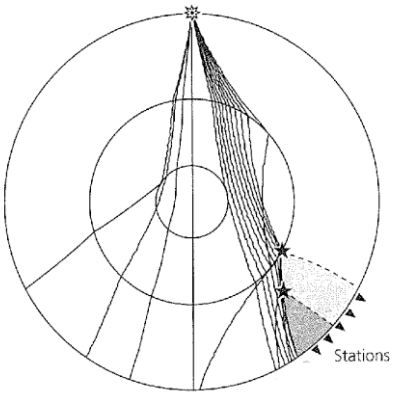

Figure 2 Propagation of body waves through a planet with a liquid outer core and solid inner core. [15]

Seismographs used in the past, namely the SEIS instrument used on the InSight lander, are capable of globally detecting R3 for seismic events of 10^{16} Nm, roughly equating to a 4.4 magnitude Earthquake. Table 1 outlines the specific instrument requirements necessary to detect R3 for seismic events of this magnitude. Seismometers are instruments able to measure extremely small vibrations, in this case vibrations on the surface of Mars. These devices contain one or more pendulums, and when the base of the device is perturbed, by a seismic event, the pendulum and device do not move synchronously due to the pendulum's inertia. This difference in motion is measured and based on the dynamic properties of the pendulum within the seismometer the magnitude of the ground perturbation can be determined. The seismograph to be used in the SAMUS mission is capable of measuring perturbations in three axes, allowing it to detect the surface (horizontal) waves and body (vertical) waves required to meet our mission objectives.

The 2013-2022 NASA Planetary Science Decadal also announced a goal to characterize Mars's ancient climate and climate processes – MEPAG goal II. Some important questions, pertaining to Martian climate modeling, outlined in this paper, include understanding how and why the Martian atmosphere evolved in the manner it did, and what processes did, and still do, control the escape of outgassing into the atmosphere. The collection of information on atmospheric phenomena over time and in different locations, allows for the determination of the forces driving these phenomena. In order further develop the climate model of Mars, the climate model results must be compared to landed meteorological data [14]. The secondary goal of the SAMUS mission is to further the understanding of the processes and history of climate on Mars. Currently the ExoMars Trace Gas Orbiter (TGO) is measuring characteristics of the gas escaping Mars's atmosphere. The SAMUS mission will attempt to assist the ExoMars Trace Gas Orbiter in its mission by collecting ground-based climate data. Specifically, the SAMUS mission will collect temperature, wind speed, pressure, and UV radiation levels, at each of our landing sites. Table 1 outlines the specific instrument requirements needed for data collection. These instruments must measure pressure, temperature, wind speed, and radiation levels over the range of ambient conditions that will be experienced on the surface of Mars.

How can measuring these atmospheric parameters help to create a model of the Martian climate? Climate modeling is a computationally and scientifically difficult task. Scientifically, these climate models evaluate and predict the interaction between hundreds of phenomena, whether it being the effect of solar radiation on the heating of the Martian atmosphere, dust storms causing the surface of Mars to cool, or even pressure and temperature differences causing carbon dioxide, a greenhouse gas, to sublimate. Computationally simulating these interactions is equally difficult, as the scope of these interactions cannot be localized to a lander, or even Valles Marineris, but to Mars and its interactions with the Sun. Climate models compartmentalize the interactions that affect climate. A specific code segment may be dedicated to the freezing and sublimation of carbon dioxide, to solar heating of the surface, and another to wind. Each of these compartmentalized sections of code, pertaining to a physical phenomenon, must be verified with physical data to be useful, and when this has been done for as many phenomena as we are able, a useful climate model may be obtained. Climate models are always wrong, as they are only approximations to the actual system. But climate models may be useful when they can provide information that would have not been present otherwise. By collecting atmospheric data at the SAMUS landing sites, we will provide a new set of information that can be used to verify localized interactions to be used in a much larger model of the Martian climate as a whole.

The atmospheric instrumentation package to be used on the SAMUS mission will be based on the Rover Environmental Measurement Station (REMS). REMS is a TLR 9 device used in previous mission to Mars, and measures atmospheric pressure, wind speed, solar radiation, and temperature. Atmospheric pressure, and wind speed are measured using a suite of pressure transducers. A pressure transducer contains a strain gauge which has electrical properties that vary based on the amount of deformation. Varying pressure causes these gauges to deform, and the resultant deformation can be determined by measuring the changes in these electrical properties – such as voltage drop across the device. Similarly, a thermocouple has electrical properties that vary depending on the temperature of the device, allowing for temperature to be measured. REMS measures UV radiation using 6 UV photodiodes that measure different portions of the UV Spectrum. These photodiodes produce a voltage depending on the intensity of UV radiation hitting the device. With a proven track record, and capable of measuring the required atmospheric parameters, REMS exactly meets the science criteria for the SAMUS mission.

The baseline science mission of SAMUS will be the deployment of a network of seismic instrumentation, and a network of atmospheric data collection instruments in proximity to the Valles Marineris. If this science mission is not able to be completed, and the mission is to be descoped, the threshold science mission of SAMUS will be the deployment of, only, a network of seismic instrumentation along Valles Marineris.

Table 1 Science Traceability Matric for the Proposed SAMUS Mission

Science/Technology Goals	Science/Technology Objectives	MR 1. Physical Parameters	MR. 2 Observables	Instrument Requirements		Projected Performance	Mission Requirements (Top Level)
Understand the origin and evolution of Mars as a geological system	Establish a network of seismic sensors to construct a seismic model of the Martian interior around the Valles Marineris. (SEIS)	Globally detect R3 for 1016 N m quakes	Seismic Waves	Horizontal	$\leq 10^{-9}$ (m/ s^2)/√Hz	$\leq 10^{-9}$ (m/ s^2)/√Hz	Locate Seismic Epicenters to within 100km
				Vertical	$\leq 10^{-9}$ (m/ s^2)/√Hz	$\leq 10^{-9}$ (m/ s^2)/√Hz	
				Vertical and horizontal (SP) [0.2-15] Hz	$\leq 10^{-8}$ (m/ s^2)/√Hz	$\leq 10^{-8}$ (m/ s^2)/√Hz	Positively identify whether recent seismic activity is a result of tectonic activity
				Vertical and horizontal (SP) [15-50] Hz	$\leq (f/15)^2 \times 10^{-9}$ (m/ s^2)/√Hz	$\leq (f/15)^2 \times 10^{-9}$ (m/ s^2)/√Hz	
				Horizontal	[0.1-1] Hz	[0.1-1] Hz	
				Vertical	[0.1-1] Hz	[0.1-1] Hz	Determine the radius of Martian core to ± 250 km
			Bandwidth	Vertical and horizontal (SP)	[0.2-50] Hz	[0.2-50] Hz	
Understand the processes and history of climate on Mars	Assist ESA-NASA Trace Gas Orbiter's climate data collection. (REMS)	Atmospheric temperature, wind speed, pressure, UV radiation	Weather Conditions	Ground Temperature	150-300 K	150-300 K	Provide auxiliary environmental telemetry to build climate model (±0.1°C, 0.1 Pa, 0.1 m/s, 200-380 nm)
				Air Pressure	1-1150 Pa	1-1150 Pa	
				Horizontal Air Speed	0-70 m/s	0-70 m/s	
				Vertical Air Speed	0-10 m/s	0-10 m/s	
				UV Determination	UVA, UVB, UVE, UVD, UVE	UVA, UVB, UVE, UVD, UVE	

Mission Implementation

Vehicle Overview

The SAMUS mission features two main systems operating in tandem, the first being an orbiter bus, and the second being a pair of identical landers. Upon launch, both landers are integrated with the orbiter bus and remain so until their deployment and subsequent arrival on the Martian surface. The overall vehicle configuration is seen in Figure 3.

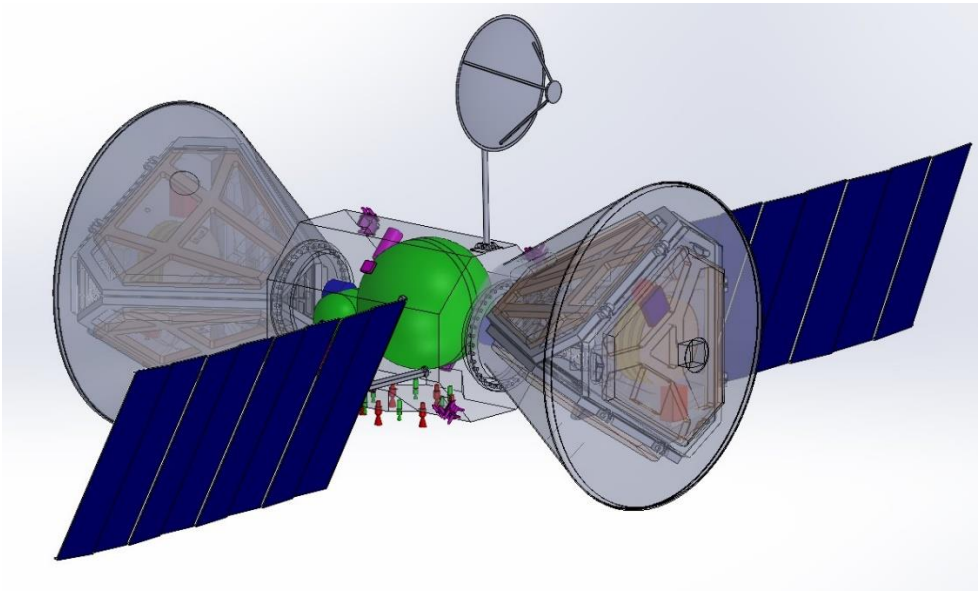

Figure 3 SAMUS overall vehicle configuration

The orbiter bus contains the propulsion system, communication system, attitude control and determination system (ADCS), and power system necessary to facilitate the arrival of the landers in their designated landing sites on the Martian surface. In addition, it provides power and communications for both landers during the interplanetary cruise until arrival and serves as a data relay between Earth and Mars over the duration of the lander's mission lifetime. The orbiter bus features two eight square meter deployable solar arrays and a deployable high gain Ka-band antenna. These deployable features enable the spacecraft to fit into the launch vehicle's payload fairing during launch. The orbiter is shown in its stowed configuration in Figure 4.

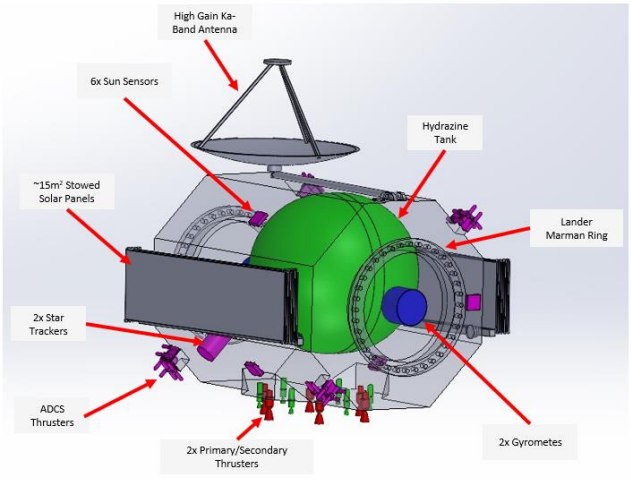

Figure 4 Stowed orbiter bus configuration

The orbiters feature an array of twelve primary thrusters running off a pressurized monopropellant system. This propulsion system provides the thrust necessary to facilitate the arrival of the spacecraft into its final science orbit and perform orbital maintenance maneuvers during normal operation. The same monopropellant system feeds twelve ADCS thrusters for station keeping and pointing operations. The orbiter's ADCS system also features reaction wheels for attitude control, and star trackers, sun sensors, and gyrometers for attitude determination.

Both landers are each integrated into an aeroshell enclosure until their arrival on the Martian surface. The aeroshell enclosure serves as a means of thermal protection during entry into the Martian atmosphere and during aerobraking maneuvers. They also house the necessary ADCS and propulsion components to navigate the landers to the Martian surface after their ejection from the orbiter bus. The aeroshell also contains a supersonic parachute that will be deployed during entry into the Martian atmosphere.

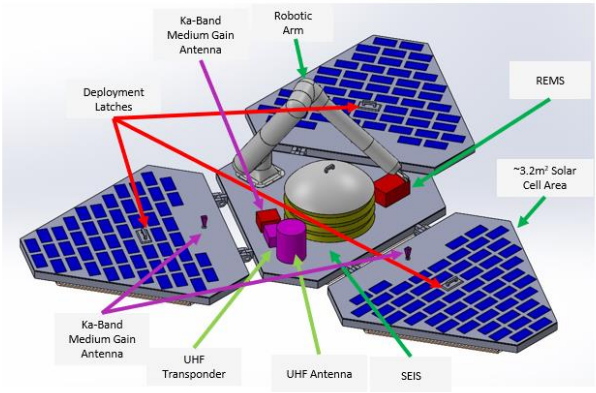

Figure 5 Deployed Lander Configuration

The landers are home to the science instrumentation necessary to carry out the previously defined mission objectives during their lifetime on the Martian surface. They are stationary during their operation, and do not include a rover. They are, however, designed with a deployable tetrahedral structure to minimize their volumetric footprint while integrated into the aeroshell (Figure 6). The landers will transition into their deployed configuration during operations on the surface. The primary features of the landers include the two primary science instruments and a robotic arm to aid in the deployment of the lander and placement of the SEIS instrument (Figure 5). During their operation on the surface, the landers are powered by a 3.2 square meter solar array that charges lithium ion batteries. The lander features an ultra high frequency (UHF) helical antenna and two Ka-band medium gain transponders for transmission of science and engineering data to Earth and relay satellites. Each petal of the lander also includes an airbag system to protect the lander during its landing upon the Martian surface. These airbags can be deflated and retracted via a winching mechanism so as not to impede the placement of the seismic instrument.

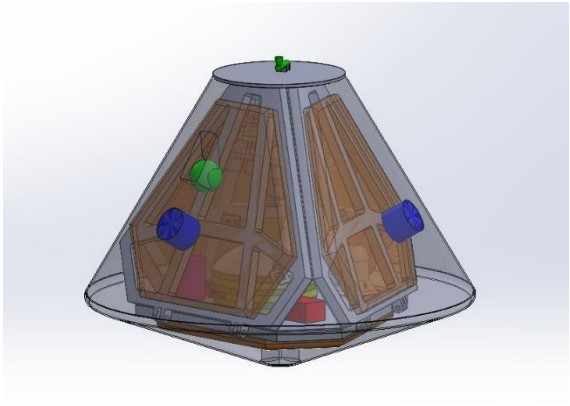

Figure 6 Stowed Lander in Aeroshell

Concept of Operations

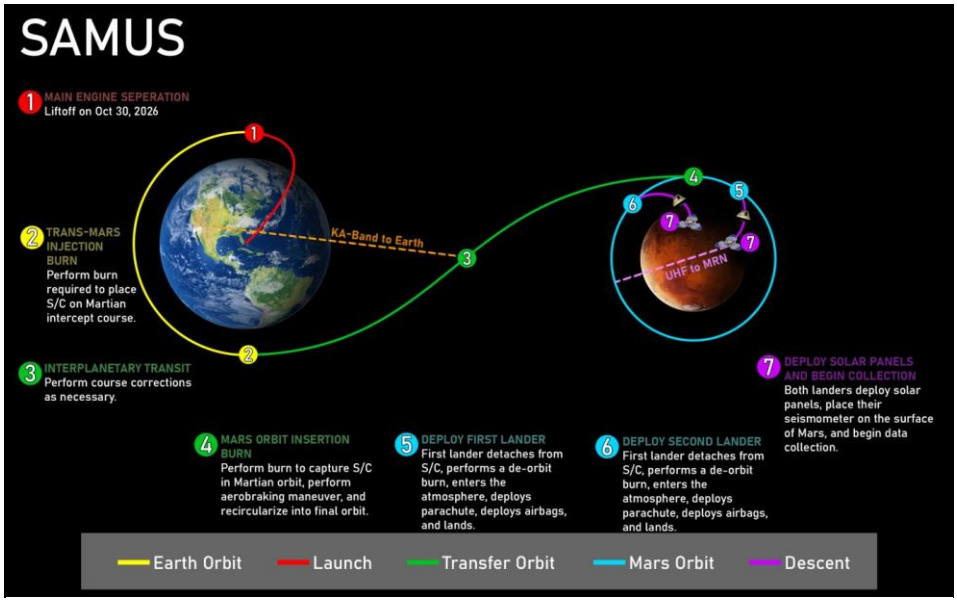

Figure 7 Concept of Operations Concept of Operations

Interplanetary Transit

The SAMUS spacecraft will launch from Earth via a heavy class launch vehicle, on October 30th, 2026. The launch vehicle will insert SAMUS directly into an interplanetary trajectory, imparting a C_3 of 9.133 km^2/s^2, at an inclination of 21.85 degrees to the ecliptic. Over the course of 295 days, the spacecraft will perform course correction maneuvers as necessary, arriving at Mars on August 20th, 2027.

Martian Orbit Insertion

Once the spacecraft has arrived at Mars, it will insert into a Martian orbit from a hyperbolic pass at a periapsis radius of 3486 kilometers. It will do so via an impulsive burn opposite to the direction of motion, with a magnitude of 0.8142 km/s. The spacecraft will inherently arrive at an inclination of 20 degrees with respect to the Mars Inertial Coordinate Frame. The resulting orbit will be 30,396 by 3,486 kilometers, having an eccentricity of 0.7942.

Aerobraking

Using the aerodynamic drag of the Martian atmosphere, SAMUS will perform an Aerobraking maneuver, taking approximately 19 weeks.

Circularization

Once SAMUS's apoapsis radius has reached 3500km, it will perform an impulsive circularization burn at apoapsis in the direction of motion with a magnitude of 0.0954 km/s. Doing so will raise SAMUS's periapsis radius to 3500km, circularizing the orbit and concluding the Aerobraking maneuver. Once in this final orbit, the ground track will phase at a rate of 30 degrees per period, with an orbit period of approximately 105 minutes.

Entry, Descent, and Landing

The two landing zones are located at 18 degrees South, 54 degrees West and 18 degrees South, 86 degrees West. To land in these regions, the landers will begin their Entry, Descent, and Landing procedure 180 degrees prior to these positions, 126 degrees East and 94 degrees East respectively. Each lander will mechanically separate from the spacecraft bus, perform an impulsive deorbit burn of 0.00283 km/s, and begin descent through the lower Martian atmosphere. Once in the lower atmosphere, each lander will deploy its parachute to slow its descent. Closer to the ground, the airbags located on each panel of the petal mechanism will inflate. Finally, each lander will touch down and begin stowing the parachute and airbags via their winch mechanisms.

Payload/Instruments

Each lander will be equipped with the same suite of instruments chosen in accordance with the specific science goals of this mission. There are four primary components vital to each lander completing its science mission: the Seismic Experiment for Interior Structure (SEIS), the Rover Environmental Monitoring Station (REMS), and a camera and robotic arm provided by Motiv Space Systems. The level 3 mass budget for one lander including this instrumentation is shown in Table 2.

Table 2 Lander Payload Level 3 Mass Budget

Instrument	Mass (kg)
1.1.1 SEIS	29.5
1.1.2 REMS	5
1.1.3 Robotic Arm	50
1.1.4 Camera with Mast	5
1.1.5 Structure	57.89

SEIS

The primary instrument on each lander will be SEIS, as this will carry out each landers' goal of observing any and all vibrations resonating within the surface of Mars. This instrument, developed by CNES, is incredibly powerful and sensitive – it is capable of tuning to tremors smaller than a hydrogen atom. In addition to bellows that sense the physical vibrations as shown in Figure 8, SEIS hosts an array of sensors that help hone-in measurements – including wind, pressure, temperature, and magnetic field sensors [12]. This array of instruments allows SEIS to not only read seismic waves cause by Marsquakes and meteor strikes, but additionally the minute vibrations caused by atmospheric turbulence such as dust devils. Moreover, SEIS is completely computationally self-sufficient, saving a large amount of complexity for data handling on-board the landers.

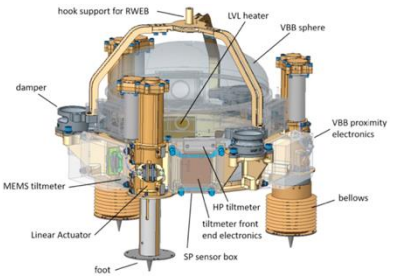

Figure 8 SEIS Breakdown

REMS

A secondary science goal of the mission is to collect data on the general climate and weather conditions of the Martian surface, which REMS will be responsible for. REMS gets its namesake from its original use case on the Mars Curiosity Rover – Rover Environmental Monitoring Station. On Curiosity, the REMS booms were mounted on the mast of the camera, as is planned for each of the landers for SAMUS. Attachment onto the mast of the telescoping cameras will provide not only vertical mobility, but easier electrical integration into the lander. The weather station will continually monitor atmospheric pressure, humidity, wind currents, and ultraviolet radiation from the Sun. Both booms are capable of measuring air temperature and wind speed and will be mounted orthogonally to each other to determine the wind currents in any horizontal direction, as shown in Figure 9. Boom 1 will measure the intensity of infrared radiation emitted from the ground to determine ground temperature, while Boom 2 will track humidity. As for pressure and UV measurements, a small so-called "chimney" implanted into the chassis of each lander will be hooked up to a pressure sensor in order to measure pressure changes, while detectors on the deck of each lander will measures the ultraviolet radiation at the Martian surface.

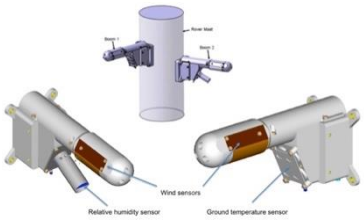

Figure 9 REMS Breakdown

Robotic Arm

A key issue in the deployment of our science instrumentation is doubly righting the lander once it lands as well as safely placing SEIS on the surface of Mars. A heavy-duty robotic arm will accomplish both these goals effectively. The preliminary design for the arm is based off the arm used aboard the Mars Perseverance Rover – a custom built mechatronic designed by Motiv Space Systems. This arm was built specifically to withstand Martian surface conditions and carries a scientific payload of 45 kg mass with a maximum reach of 2.1 meters. For the SAMUS mission, the arm must only be capable of lifting the SEIS instrument which has a mass 29.5 kg, allowing us to scale down the arm to conserve on development costs as well as overall lander mass. On initial deployment – if the lander were to land on one of its 3 sides – the arm may be used apply the force needed to push the downward facing panel out and thus turn the lander upright. After this, the arm will be used to deploy SEIS in an appropriate area around the lander. Once this is complete, the arm will remain mainly stagnant, with the exception being that it may be used to close the solar panels of the lander if REMS begins to detect weather conditions which may prove hazardous to the lander – namely dust storms. The arm may also be used to shake solar panels in order to rid them of dust.

Telescoping Camera

Another vital part of the mission is being able to qualitatively determine an appropriate area to place SEIS, as well as to observer the general condition of the lander over time. A telescoping camera place centrally will accomplish both of these goals. As with the robotic arm, the camera will also be designed after the one used on the Mars Perseverance Rover, as its camera was also made my Motiv Space Systems. Utilizing the same company for the two instruments which require research and development is vital for reducing costs and ensuring ease of system integration. The camera on Perseverance – known as MastacamMars - contains a mechanical zooming and focusing mechanism; however, since the camera for SAMUS will only need to observe the lander itself and the surrounding

area, these functionalities will not be needed. The camera requirements for each lander will be the bare bones of the MastacamMars, reducing complexity of the equipment as much as possible.

Power

For our mission we have two separate power subsystems, one located on the bus and one located on each of the landers. Both the bus and landers utilize very similar systems as they produce power via solar arrays connected to the systems and store power using batteries for when the system is in eclipse. These systems are derived from the power needs of the other subsystems existing on each respective body, as the driving factor for size for our bus power system is communication and the ability to power the landers batteries, while the lander's driving force is our mission objective to have the capability to power payloads continuously.

For our specific mission the chosen materials for the solar array were multijunction Gallium Arsenide (GaA) solar cells and a nickel hydrogen battery. When choosing the solar cell material for our mission a very desirable trait for the cell to have is a very high efficiency, as for the bus this will help minimize the size of the solar panels reducing weight and cost and for the lander this will maximize the power draw during sunlight hours minimizing the size and amount of batteries needed on board. The cells themselves were found to have an area of 0.0036m^2 and can reach efficiencies of up to 29% with a degradation rate of only 2.75% a year [18], with a density of $5320\frac{kg}{m^3}$ at an average cell thickness of 150μm to give a weight of $0.798\frac{kg}{m^2}$, and coupled with the substrate and thin metal sheets holding together the panels comes to ~$3\frac{kg}{m^2}$ [5]. For our batteries a large driving factor for choosing nickel hydrogen cells was our missions need of a battery that can withstand many lifecycles, as we plan on having the bus lifecycle to end after three years and for the landers to operate for two years. Nickel Hydrogen batteries have been found to run efficiently at a depth of discharge of up to 0.5 for almost 20,000 cycles, has a conversion efficiency to appliances of 0.85, can hold a charge of 35A-hr, has a power density of $75\ \frac{Whr}{kg}$, and each cell has a volume of 0.0009m^3 [18]. A Nickel hydrogen battery has been used in multiple prior deep space missions so is a proven battery source, and one of the reasons for this is that the cells can be fitted in series to produce a single pressure vessel (SPV) that allows for greater watts to be stored and will produce the necessary 28VDC to run all of the equipment on both the bus and the landers.

Having the specific type of solar used for this mission we can now calculate the amount of energy each individual solar cell will be able to produce for both the bus and the lander. This will be done using Equation 1 below

$$P_{sc} = A_{sc}\eta_{deg}\eta_{cell}\eta_{point}S(R_c) \tag{1}$$

The area of our solar cells was defined by choosing which material to use for the solar array. The efficiency of the solar cell also came from the chosen material and was found to be 0.29 for both the bus and lander. The only other variable constant between the bus and lander is the solar irradiance that exists at Mars. This is found using the solar irradiance at Earth, which is $1366.1\frac{W}{m^2}$, and a ratio of 1AU over the distance to the location in question in AU. Using this the solar irradiance at mars is $591.2829\frac{W}{m^2}$ which is consistent with measured values. The first value to differ for the bus and lander is the degradation efficiency of the solar cells. Both systems degrade at a rate of 2.75% per year, however the bus us designed to run for three years while the landers meet the end of their lifecycle at 2 years. Using these values, the degradation efficiency for the bus and landers are 0.9197 and 0.9458, respectively. The final value is the pointing efficiency of both of these systems. The bus pointing efficiency was found taken into account that there are sun sensors on the bus that will allow the solar arrays to be pointed at the sun throughout the cruise stage. Even with the use of the sun sensors, a pointing efficiency of $\cos(25°)$ is used in order to compensate for any deviations from the optimal angle. For the lander the pointing efficiency has to take into account multiple factors; the latitude in which the landers touch down, the angle the solar panels are on the ground, and the average angle received over the sunlight period. Both landers are located at 18 degrees south, which is greatly beneficial to their pointing efficiencies as they are close to the equator. The terrain of their landing sites is very flat, which ties well with location near the equator as the panels do not need to be angled in order to receive their maximum pointing efficiency. Finally, taking into account the average angle of incidence for the duration of the sunlight period the efficiency angle of the landers was set to be $\cos(50°)$. Using all of these values the bus and lander solar cells were found to produce 0.4613W

and 0.3701W, respectively, which taking into account the size of each solar cell gave the solar array configurations for the bus and lander a power output of $128.1484\frac{W}{m^2}$ and $102.8094\frac{W}{m^2}$, respectively.

A breakdown of all other subsystems and their power requirements is necessary to determine the scope of how many batteries may be needed and how large the solar arrays for our craft will be. Creating a power budget breakdown of each subsystem is a very effective and efficient method of doing this. A power budget was created for both the bus and the landers and are shown below in Tables 3 and 4**,** respectively. For both of these budgets the maximum power output of each subsystem that could possibly run simultaneously was taken into account so as to not cripple the spacecraft or lander in case of an emergency. Both power budgets show down to level three subsystems for power consumption specificity

The summed wattage of all the components was necessary to find the final area of the solar array as well as how many batteries are needed to power the bus and landers throughout their entire respective mission lifecycles. Using the values from the tables above we can find just how many watts the lander and bus needs to run while in an eclipse. Incorporated into our equation is also enough charge in the batteries to power the lander communications devices for two ten-minute link times. Using Equation 2 below we can solve for the necessary W-hr needed to power the equipment throughout their respective eclipse times.

$$C_{bat} = \frac{1}{(DOD*\eta_{conv})}\sum_{k=1}^{q} P_k T_k \tag{2}$$

The nickel hydrogen batteries used in this mission hold a can hold 980 W-hr for our specific voltage and using these values the bus only needs one battery while the landers need three batteries each to keep their instruments running throughout the night. Now having the necessary power required to charge the batteries the solar array sizes can now be accurately found. Equation 3 below gives the power in watts the solar array needs to produce during sunlight periods.

$$P_{SA} = \frac{\sum_{k=1}^{n} \frac{P_k T_k}{X_k}}{\sum_{k=1}^{r} T_k} \tag{3}$$

Taking this value found for both the bus and the lander and then dividing it by their respective $\frac{W}{m^2}$ values found above, we were able to solve for the total solar array area necessary for these two systems, which came out to be 14.6268m^2 for the bus and 3.1680m^2 for the landers. Using these values in the power budget gave us the margins found above, which for both systems falls within 25-35% which is a reasonable value for a Pre-Phase A mission.

The final area to note for our systems is that the ADCS and the robot arm payload for the landers are not listed inside of their power budget tables. This is because both of these structures have a designed mission purpose of being used only during descent and landing. Due to this, both of these systems will be powered by the batteries stored on the landers, and as such a power increase can be found in the bus power budget as it now is responsible for recharging the lander batteries before descent as the self-discharge at a rate of 10% per month and will be depleted after the cruise stage.

Table 3 "Level 3" Power budget for the lander system.

Lander Power Budget				
	Level 2 and 3			
Element	**CBE**	**Cont**	**Allocated**	**Level 1**
1.0 Payload				9.713
1.1 SEIS	8.5	10.00%	9.35	
1.2 REMS	0.33	10.00%	0.363	
2.0 Spacecraft Bus				209
2.1 Propulsion	0	10.00%	0	
2.2 ADCS	0	10.00%	0	
2.3 Communications				
2.3.1 Small Deep Space Transponder	20	10.00%	22	
2.3.2 UHF Transceiver	20	10.00%	22	
2.4 C&DH				
2.4.1 RAD750 Processor	10	10.00%	11	
2.5 Power				
2.5.1 Nickel Hydrogen Batteries	80	10.00%	88	
2.6 Structure	0	10.00%	0	
2.7 Thermal Control Systems				
2.7.1 Kapton Heaters	60	10.00%	66	
3.0 Spacecraft Allocated Power				218.713
4.0 Margin				32.70%
5.0 Total Power Available				325

Table 4 "Level 3" Power budget for the bus system.

	Level 2 and 3			
Element	**CBE**	**Cont**	**Allocated**	**Level 1**
1.0 Payload				396
1.1 Lander (x2)				
1.1.1 Nickel Hydrogen Batteries	180	10.00%	198	
2.0 Spacecraft Bus				979.176
2.1 Propulsion				
2.1.1 MR-104J Valve Heater	6	10.00%	6.6	
2.1.2 MR-104J Cat. Bed Heater	26	10.00%	28.6	
2.1.3 MR-104J Valve	56	10.00%	61.6	
2.1.4 MR-106L Valve Heater	4	10.00%	4.4	
2.1.5 MR-106L Cat. Bed Heater	7.06	10.00%	7.766	
2.1.4 MR-106L Valve	25.1	10.00%	27.61	
2.2 ADCS				
2.2.1 VRW-D6 Reaction Wheel System	110	10.00%	121	
2.2.2 MRE-1.0 Monopropellant Thruster (x12)	180	10.00%	198	
2.2.3 Astrix 90 Gyrometers (x2)	27	10.00%	29.7	
2.2.4 Ball Aerospace CT-2020	24	10.00%	26.4	
2.3 Communications				
2.3.1 Small Deep Space Transponder	20	10.00%	22	
2.4 C&DH				
2.4.1 RAD750 Processor	10	10.00%	11	
2.5 Power				
2.5.1 Nickel Hydrogen Battery	200	10.00%	220	
2.6 Structure	0	10.00%	0	
2.7 Thermal Control Systems				
2.7.1 Kapton Heaters	195	10.00%	214.5	
3.0 Total Power Required				1375.176
4.0 Margin				26.66%
5.0 Total Power Available				1875

ADCS

The ADCS performance requirements for the SAMUS mission are derived from only two major mission functions, these mission functions being maintaining an optimal solar panel orientation with respect to the sun and reorienting the spacecraft after the Mars orbit circularization burn to prepare for the two lander de-orbit burns. With a lander placed on either end of the spacecraft bus, the bus must complete a 180-degree rotation about its largest moment of inertia within the time period of a few orbits. Due to having two landers, this spacecraft is quite massive and will have a large moment of inertia. This large moment of inertia, paired with the large changes in orientation required for lander ejection, means that a spin-stabilized system will not be efficient with respect to propellant use, time to reorient, nor offer the orientation accuracy required for lander ejection. A three-axis attitude control scheme does increase complexity and cost of the craft, but it is more optimal for the maneuvers required throughout this mission. For these reasons, a three-axis attitude control scheme will be used.

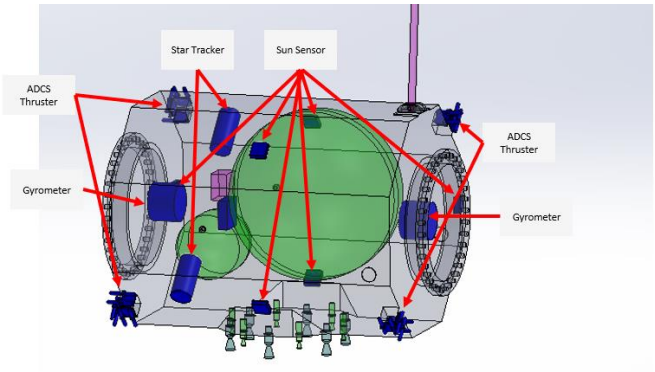

Figure 10 Location of ADCS Components

Attitude determination for this craft will be achieved through the use of star trackers, gyrometers, and sun sensors (Figure 10). The fusion of data output by these sensors will offer continual knowledge of the spacecraft attitude. This attitude determination sensor fusion will consist of a course fast loop, periodically corrected by fine slow loop. At slow rotation rates, the star trackers will provide accurate attitude information at a slow rate, thus making up the slow loop. The gyrometers will integrate change in attitude in the fast loop, using the slow loop's accurate attitude information to continually correct for drift in the gyrometers sensors. On startup, and before starting the attitude determination loop, sun sensors will be required to obtain an estimate of attitude in order for the star trackers to determine attitude. The resultant output is a fast and accurate stream of attitude data. Figure 11 shows this operation loop graphically.

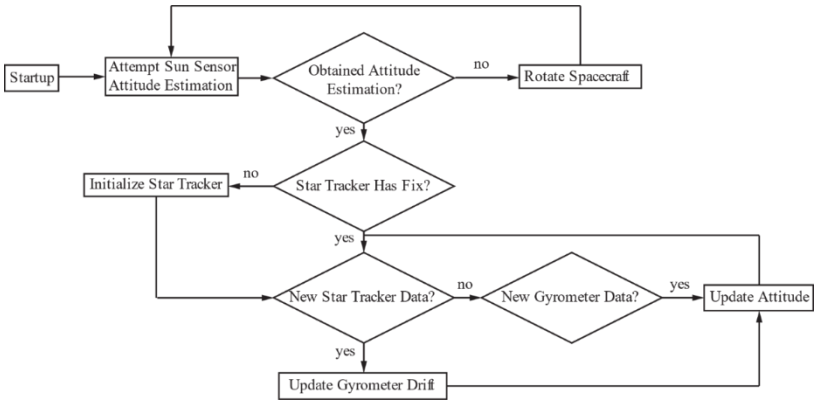

Figure 11 Attitude Determination Startup and Operational Loop Visualization.

In the event of a power cycle, the spacecraft needs to be capable of obtaining a rough attitude estimation with no prior knowledge of current attitude. This is achieved by placing sun sensors on the craft such that the sun can be located in any spacecraft orientation. The sun sensors chosen for the SAMUS mission are the Sat Search CSS. These sensors offer a 180-degree measurement FOV, with a maximum ± 3 degrees accuracy. A 180-degree measurement FOV allows for an initial attitude estimation to be made with just six Sun sensors, while still offering some level of redundancy in the event of a sensor failure. The level of redundancy will be dependent on the location of the sensor failure because obstruction of the Sun sensors will be inevitable – solar panels, landers, and communication equipment may obstruct line of sight to the Sun. In the event of multiple Sun sensor failures and obstruction of line of sight to the sun, a searching maneuver will rotate the space craft until operational Sun sensors can make an initial estimation of spacecraft attitude.

After an initial attitude estimation is made, a pair of Ball Aerospace CT-2020 star trackers will begin operation. Each sun sensor will ideally be pointing perpendicular to the Solar System Ecliptic. However each Sun sensor is capable of operating at full performance with a 33-degree Sun angle. In the event of a star tracker sensor failure, a single sensor is still capable of determining attitude of the spacecraft to <1.5 arcsec when nearly non-rotating

and maintaining tracking up to eight degrees per second with reduced performance. In the event of rotation exceeding eight degrees per second, two redundant Astrix 90 gyrometers are able determine attitude if a previous attitude measurement and rotation is limited to 60 degrees per second. The maximum expected rotation is not to exceed one degree per second –this requirement is derived from the required 180 degree turn in the span of a single orbit at a Martian orbit altitude of 500km. Gyrometers alone cannot determine the attitude of the system without periodically correcting for drift using data obtained from the onboard star trackers. The maximum gyrometer drift is 0.3 degrees/hour, meaning sub degree attitude accuracy can be achieved without bias correction for over three hours.

With very generous moment of inertia estimations, 5000 kg-m^2 about minor axes and 3000 kg-m^2 about the major axis, a maximum necessary change in momentum throughout three Martian orbits of 5.68 N-m-s is determined with a factor of safety of four. The maximum torque requirement for the spacecraft in Martian orbit is 4.67 mN-m. Control function will be handled majorly by the VRW-D-6 reaction wheel system. This four-reaction wheel system can impart a maximum of 6 N-m-s before reaching the maximum spin speed of 6000 rpm, meeting the maximum angular momentum requirement mentioned previously. This system can also impart a maximum torque of 90 mN-m, which meets the mission criteria with a large margin. If reaction wheels are nearing maximum spin speed, a series of thrusters will fire in order to desaturate them. The thrusters used for attitude control are the Northrop Grumman MRE-1.0, with a specific impulse of 218 s^{-1}. These thrusters can impart a minimum impulse of 0.018 N-s and produce a minimum of 3.4 N of thrust. With thruster placement roughly one meter from the center of mass, complete desaturation of the reaction wheels can be achieved without risk of overcorrection. With the spacecraft performing aerobraking burns for 18 weeks, an overestimate of 1512 orbits are required. If the spacecraft were required to desaturate the reaction wheel system once an orbit, a total propellant mass of 8.5 kg is required. 30 kg of propellant is allocated to account for the interplanetary transfer and to increase margin. The total level three mass breakdown of this bus subsystem can be seen in Figure 5.

Table 5 Level 3 Top Down ADCS Mass Breakdown

	Level 3			Level 2
	CBE	Cont.	Allocated	
2.2.0 ADCS				77.148
2.2.1 VRW-D-6 reaction wheel system	3.00	20%	3.6	
2.2.2 12x Northrop Grumman Thruster	9.00	20%	10.8	
2.2.3 2x Astrix 90 Gyrometers	9.00	20%	10.8	
2.2.4 2x Ball Aerospace CT-2020	12.00	20%	14.4	
2.2.5 6x Sat Search CSS	1.29	20%	1.548	
2.2.6 Propellant	30.00	20%	36	

Because the SAMUS spacecraft contains two landers that do not share a common landing site, the bus cannot be used to de-orbit the landers. Each lander must be capable of independently determining and controlling attitude, and deorbiting. The unique attitude and control requirements of the landers allow for an ADCS solution much less complex than what was seen on the spacecraft bus. The landers only require attitude information and controlled thrust during the de-orbit burn. In order to obtain the attitude of the spacecraft bus, sun sensors, star trackers, and gyrometers were required. However, because the landers only need attitude information for less than an hour, gyrometers alone can be used. Before a lander is ejected, attitude information from the spacecraft bus will be sent to the lander. With this attitude information, two – one for redundancy – Astrix 90 gyrometers onboard the lander will be utilized for attitude determination throughout the de-orbit burn. With attitude determined, control will be achieved with a VRW-D-6 reaction wheel system. Attitude control is only required to maintain the desired thrust vector to deorbit the lander, therefore desaturation of the spacecraft will not be necessary.

Propulsion

The SAMUS mission requires 2 separate propulsion systems: one for the bus and one for the landers. The propulsion system for the landers is like that of the bus system, both being pressure-fed, monopropellant hydrazine systems. This system was chosen for the bus in order to fulfill the mission ΔV requirement of 0.9096 km/s, while minimizing complexity and propellant mass. A similar system also fulfilled the ΔV requirement for each lander of 0.107 km/s. Both systems meet the impulsive burn requirements for the mission, where the major impulsive constraint comes from the deorbit burn for the landers. An impulsive burn limit of 10 percent the circular orbit was chosen which comes out to be 630 seconds, much larger than the theoretical burn time of 97 seconds.

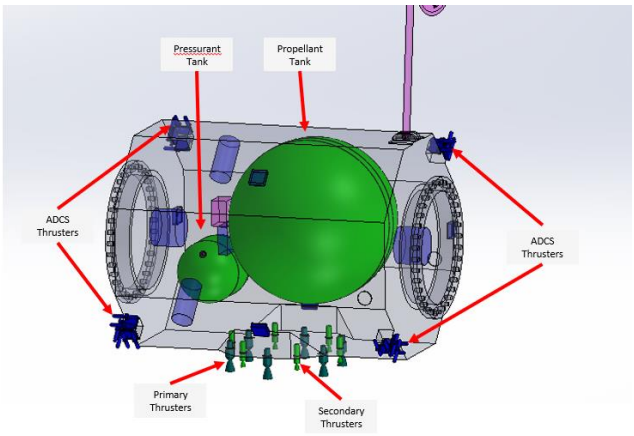

Figure 12 SAMUS Bus Propulsion System

Using the Mars Reconnaissance Orbiter's 20 thruster propulsion system as inspiration, the SAMUS bus uses a primary thruster array, secondary thruster array, and 12 dedicated ADCS thrusters (Figure 12). The primary thruster array is made up of 6 MR-104J thrusters from Aerojet Rocketdyne. The primary array has a thrust of 3650 N and a specific impulse of 231 seconds. For the secondary thruster array, there are 6 MR-106L thrusters from Aerojet Rocketdyne. The secondary array has a thrust of 192 N and a specific impulse of 232 seconds. Both thruster arrays perform the Mars insertion burn, and the secondary thruster array performs the trajectory correction maneuvers. In order to provide the twenty-four thrusters with propellant, the bus is fitted with both a Northrop-Grumman model 80507-3 propellant tank and model 80536-1 pressurant tank. This allows the system to operate at 2757.9 kPa, on the high end of the operating pressure for the primary thruster array. With the burn requirements in addition to the attitude correction burns, the bus has a required propellant mass of 213.8971 kg. After accounting for ullage and residuals in the propellant tank, there is a

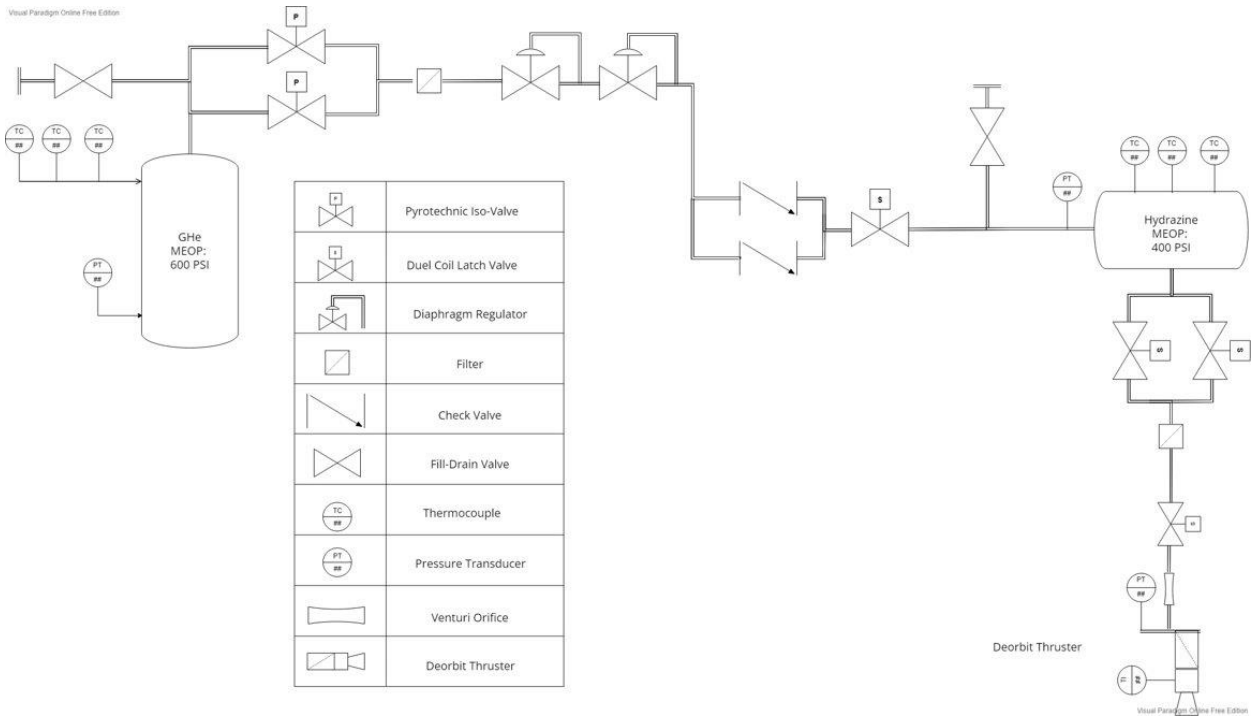

Figure 13 P&ID for the Landers

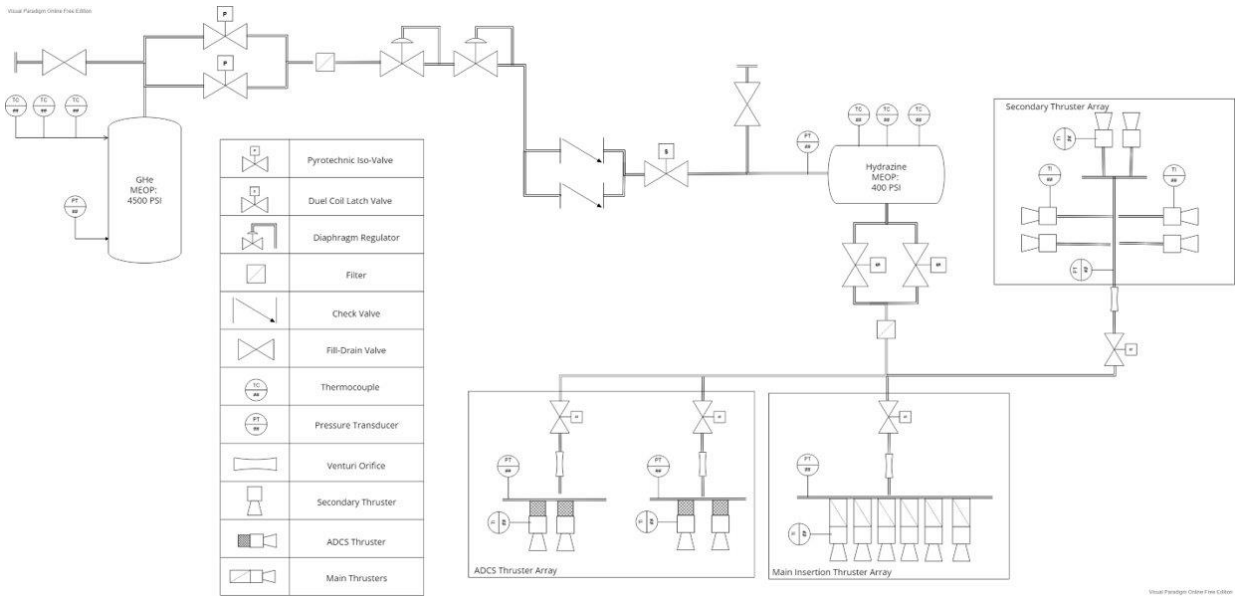

Figure 14 P&ID for the Spacecraft Bus

total propellant mass of 1377.77 kg which makes for a 13.5 percent propellant margin. The piping and instrumentation diagram for the spacecraft bus is pictured below in Figure 13.

For the landers, each is fitted with a single MR-107T thruster from Aerojet Rocketdyne. This thruster provides 100 N of thrust and a specific impulse of 220.5 seconds. The propellant deliver for the landers consists of both a Northrop-Grumman model 80421-1 propellant tank and model 80119-105 pressurant tank. This gives the same operating pressure as the bus of 2757.9 kPa. The lander's propulsion system is tasked with the deorbit burn to put the landers onto Mars' surface. This burn gives the lander a required propellant mass of 6.082 kg. The total propellant mass for each lander after ullage and residuals is 9.39 kg, giving a propellant margin of 54.4 percent. The piping and instrumentation diagram for the lander is shown in Figure 14.

Communications

The communications subsystem for the SAMUS mission is designed to optimize communication directly to Earth's Deep Space Network (DSN) during transfer and orbit maneuvers and from the surface of Mars, as well as data relay from Mars surface. The subsystem on the spacecraft bus is comprised of a primary high-gain antenna with Ka-band operating capability, two Ka-band low-gain antennas, and a small deep-space transponder to command modulation/de-modulation, filtering, and Ka-band excitation. The lander's communication subsystem utilizes an ultra-high frequency (UHF) transceiver and UHF antenna for data relay from the surface of Mars through the Mars Relay Network. For the lander's direct-to-Earth communication, two medium-gain Ka-band antennas are employed, with a small-deep transponder on each lander.

<u>Spacecraft Bus Communications</u>

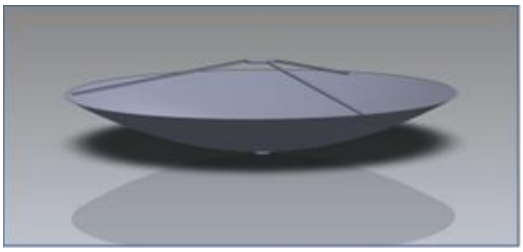

Figure 15 High-gain Ka-band antenna

The primary high-gain parabolic antenna is employed for Ka-band communications to one of the DSN's 34-meter antennas. Ka-band is utilized due to its higher allocated frequency range (34.2-34.7 GHz for uplink, 31.8 GHz-32.3 GHz for downlink), which will allow for higher rates of data transmission [4]. The 1.2-meter diameter high-gain antenna, as shown in Figure 15, is deployed after launch and provides high-rate communication to and from the DSN throughout the spacecraft bus's transit, Mars orbit insertion, and lander deployment. Figure 16 shows the mission's critical events such as these and the associated telemetry coverage approach to ensure data recovery in the event of an anomaly.

Critical Event	*Requirement*	*Objective*	*Critical Telemetry Approach/Implementation*
Separation from launch vehicle	Monitor and downlink to ground station and record spacecraft telemetry coverage during all events where failure would result in failure to meet mission objectives to assure data is available off of the flight system to support mission operations and anomaly investigations to prevent future recurrence. (*)	The spacecraft bus must downlink critical telemetry data for support or investigation purposes in case of anomaly.	At a minimum, data downlink through spacecraft bus' low-gain Ka-band antennas to 34-m DSN antenna at a rate of at least 10 Mbps.
EDL sequence + main burns			At a minimum, data downlink through spacecraft bus' low-gain Ka-band antennas to 34-m DSN antenna at a rate of at least 10 Mbps.
Lander separation from spacecraft bus			At a minimum, data downlink through spacecraft bus' low-gain Ka-band antennas to 34-m DSN antenna at a rate of at least 10 Mbps.
Deployment of solar panels & beginning of data collection		The lander must downlink critical telemetry data for support or investigation purposes in case of anomaly.	At a minimum, data downlink through UHF relay at a rate of at least 10 kbps

Figure 16 *NPR 8705.4A

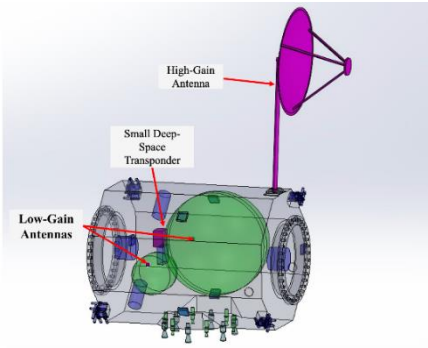

Figure 17 Location of COM Components

The two omni-directional antennas are employed for communication during critical events and emergencies at a lower data transmission rate. These Ka-band low-gain antennas are integral to transmitting and receiving communications in case the high-gain antenna is not pointed at Earth. Shown in Figure 17, the low-gain antennas are configured to remain in operation independently from the high-gain antenna in case of failure or other impediments to communication via the high-gain antenna. The small deep-space transponder (SDST) uses Ka-band radio frequency to provide transmission and reception functions, as well as perform telemetry modulation and support Ka-band downlink. Additionally, the SDST is equipped to support interactions via a MIL-STD-1553 data bus, aligning with the communications/command and data handling system architecture for the mission.

Lander Communications

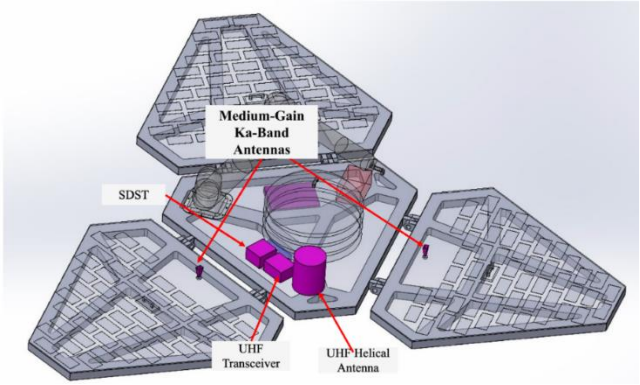

Figure 18 Lander Deck Telecommunications Configuration

The landers utilize both Ka-band and UHF communications through descent and data collection from the surface of Mars. The landers employ a pair of medium-gain antennas for Ka-band communication to the DSN 34-meter ground station. These antennas, shown in Figure 18, communicate data directly to Earth and also serve as backup to the primary UHF data relay used by the lander. The landers use a helical UHF antenna, also shown in Figure 18, to relay data to Earth through the Mars Relay Network. From Mars' surface, the UHF antenna located on the deck of the lander transmits science data to Mars Relay Network orbiters for approximately ten minutes every six hours. The lander will carry the Electra Lite UHF transceiver as Government-Furnished Equipment (GFE). The Electra Lite transceiver is to transmit, receive, and process signals, enabling the data links between the lander and relaying orbiters. In the case that the SAMUS mission qualifies for this MEP-provided payload, an implementation plan for the UHF relay system is outlined in Figure 19.

For UHF and Ka-band communications on both the spacecraft bus and the lander, conformance to bandwidth limits is necessary for implementation of the communications subsystem configuration. The allocated frequency bands for Ka-band downlink are 31800 to 32300 MHz and 390 to 405 MHz for UHF downlink [4]. The link budget for the antennas on the spacecraft bus and landers and their downlink frequencies is shown in Figure 20.

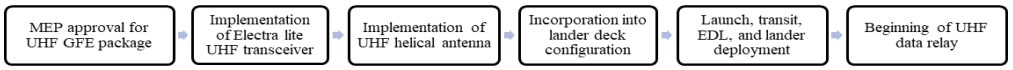

Figure 19 UHF Relay Package Implementation

Parameters	UHF LGA to MRN	HGA (Ka)	LGA (Ka) (2)	MGA (Ka) (2)	Units
Frequency	400	32300	32300	32300	MHz
Bandwidth	15	500	500	500	MHz
Transmitting Antenna Gain	1.64	50	1.64	11	dBi
Receiving Antenna Gain	12	68.2	68.2	68.2	dBi
Space Loss	-148.9	-162.6	-163.2	-175.3	dB
Atmospheric Loss	3	1	1	3	dB
Input Power	10.5	12	12	12	dBW
Received Power	178.2	728.8	245.8	349.5	dBW
E_b/N_0	11.04	18.47	15.85	13.14	dB

Figure 20 Link Budget

TPS

The thermal protection system (TPS) on both the SAMUS landers and orbiter serve to maintain temperature and provide climate control for all on-board components and instruments (Figure 21). The TPS is designed to maintain the spacecraft and landers at an overall colder operating temperature using passive thermal protection systems while using active thermal protection methods to provide localized heat to keep specific components at their operating temperatures.

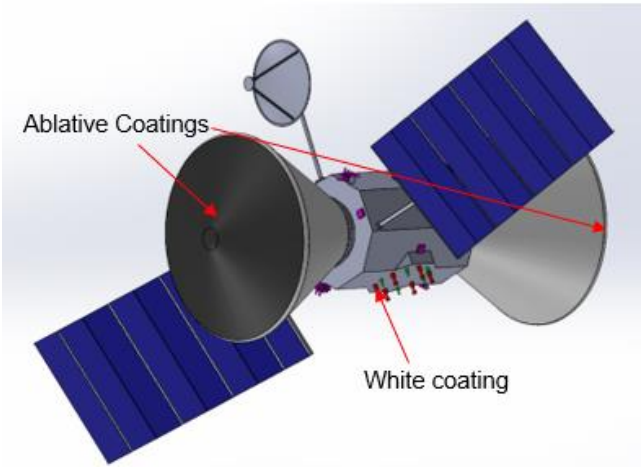

Figure 21 Orbiter & Lander Thermal Protection Systems

Orbiter Thermal Protection System

There are two main requirements the thermal protection system on the SAMUS orbiter need to complete. First, the orbiter must survive the cold nighttime and hot sunlit environments during its orbit around Mars. Second, it must do so with minimal impact on the spacecraft's weight and power. To conserve these resources, the desired spacecraft temperature during sunlit conditions was decided to be around 10°C. At this temperature, most components on the SAMUS orbiter would be operating within their design temperatures and would require no additional heat or radiators. To estimate the spacecraft temperature, an energy balance between direct solar radiation, reflected sunlight, blackbody radiation from Mars, internally generated heat, and net energy radiated into space was used. Equation 4 shows this relationship.

$$Q_{sun} + Q_{albedo} + Q_{BB} + Q_{internal} = Q_{space} \quad (4)$$

Using the above energy balance, Hughson White Paint A-276+1036 ESH UV coating was selected as the most effective coating that would provide the desired 10°C spacecraft temperature. This coating has a high emissivity factor of 0.88 and an absorption factor of 0.44. The exact spacecraft temperature calculated using Equation 4 was 10.08°C. During nighttime conditions, the minimum temperature aboard the spacecraft was calculated to be -91.8°C.

This design choice was intentional as the solar panels and communication hardware would all be functional at this temperature. All other components (batteries, gimbals, star trackers, IMUs, C&DH hardware) will be kept at operational temperatures using Kapton patch heaters.

Lastly, the orbiter's helium pressurant gas and hydrazine fuel will be kept at operating temperatures using multi-layered insulation (MLI) such as a coated and backed Kapton outer layer, goldized Kapton reflectors with Dacron netting as a separating layer.

Lander Thermal Protection System

There are also two main requirements the TPS on the SAMUS landers need to complete. First, the landers must survive re-entry through the Martian atmosphere prior to landing. Second, the landers must survive Martian climate during both daytime and nighttime conditions.

The lander thermal protection system similarly uses Hughson White Paint A-276 but will not use its 1036 ESH UV variant, which has a lower absorption rate. This is to prevent the landers from over-heating during daytime conditions on Mars. This is due to Mars' thinner atmosphere allowing less heat to be dissipated through convection and more through radiation. Similar to the orbiter, Kapton patch heaters will be used to keep the batteries, C&DH hardware, and robotic arm at operating temperatures. A 10-layer aluminized Mylar/Dacron net MLI will be used to insulate all components on the lander. However, the SEIS and REMS will not be insulated as they are designed to operate well above and below the maximum and minimum expected temperature on the lander.

Lastly, the landers will use a heat shield with a charring ablator, AVCO-5026-H/CG, which was used for re-entry on the Apollo command module. This proven method should provide a safe re-entry for each lander.

Command & Data Handling

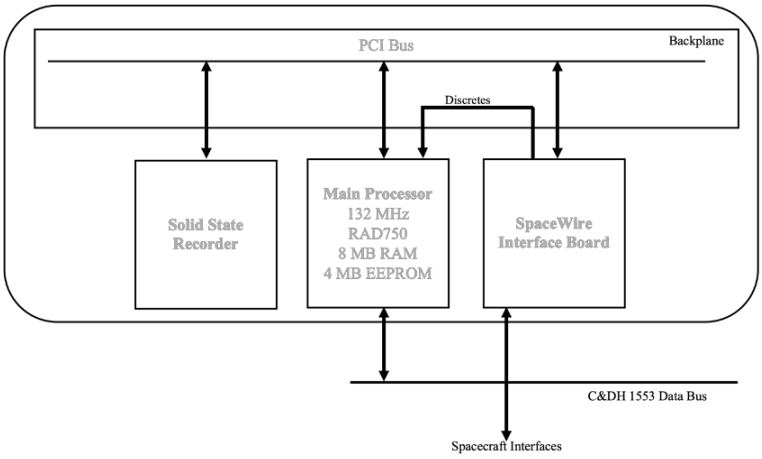

Figure 22 C&DH Computing Module Architecture

The command and data handling (C&DH) subsystem of the SAMUS mission is comprised of a radiation-hardened single-board computer, interface units, and solid-state recorders for data storage (Figure 22). The C&DH unit of the spacecraft bus and landers utilize two redundant computers of which the RAD750 is the main processor. The RAD750 operates at a speed of 132 MHz and contains 36 MB of Static Random Access Memory (SRAM), 4 MB of Erasable Programmable Read Only Memory (EEPROM), and 64 MB of Start Up Read Only Memory (SUROM), all of which are essential for storing code needed for flight software and command. The computer executes software in its VxWorks real-time operating system, with software written in C and C++. The computer also provides a 4-port SpaceWire data bus, which will be used for interface with instrumentation. The main processor is the bus controller for the C&DH 1553 data bus for instrumentation and subsystems including power and propulsion. Figure 22 shows a breakdown of the computer module at the heart of the C&DH subsystem. A solid-state data recorder for science and command data storage is included in the C&DH subsystem. Figure 23 shows a block diagram breaking down the communications and C&DH systems.

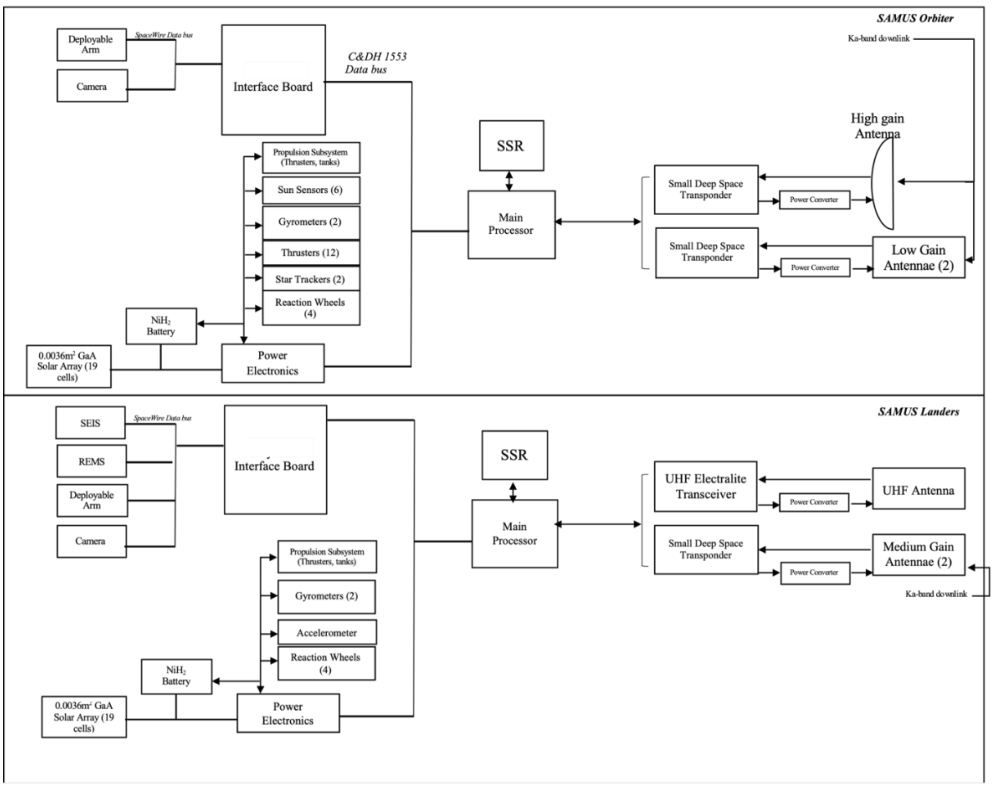

Figure 23 Communications/C&DH Block Diagram

Throughout the mission, scientific data will be stored and transmitted to Earth, and as new critical data is stored, previous data that has already been transmitted to Earth will be overwritten in the C&DH solid-state recorders. Figure 24 shows a science data collection and downlink schedule derived from the lander's instrumentation [13]. Figure 25 shows a Level 3 mass breakdown for the communications and C&DH subsystems.

Instrumentation	Data Transmission	Downlink via relay
SEIS	~600 Mbits/sol reduced to ~30 Mbits/sol	>90 Mbits/sol
REMS		
Camera	>20 Mbits/sol	

Figure 24 Data downlink schedule

Integral to management of science data collected during the SAMUS mission is a plan for archiving and transferring raw and reduced data generated during the mission to the Planetary Data System (PDS). A ground data system will process raw science data and generate science data products, as well as processing telemetry and other data. The system is responsible for supporting data analysis, validation, documentation, and archival of the science data products generated [1]. In the creation of the archive, datasets must be formatted to adhere to PDS standards. After formatting of data, the archive must be validated to ensure conformance to PDS requirements and adequacy of science data. The archive will be further supported by internal and external review and delivered to the PDS. Considerations for this data management and archiving plan are allocated in the C&DH cost estimate for the mission.

COMMUNICATIONS	
Component	**Mass (kg)**
HGA	30
LGA (2)	2
SDSTs (3)	9.6
UHF Antenna	1
UHF Electra Lite Transceiver	3
MGA (2)	1.8
Other	5
Total	52.4
COMMAND AND DATA HANDLING	
Component	Mass (kg)
Computing Module (3)	4.76
SSRs (3)	6
Other	5
Total	15.76

Figure 25 Comms/CD&H Level 3 Mass Breakdown

Structure

The structure for SAMUS can be broken down into two major parts: the lander structure, and the orbiter structure. The primary purposes of the orbiter structure are to provide an interface for each of the landers while they are stored in their aeroshells and to provide a structural bus for mounting all hardware necessary for orbital operations. The primary sizing considerations for the orbiter structure are the volumetric constraints of the internal components and the loads experienced during launch and the aerobraking thrust maneuvers. The landers interface with the orbiter bus structure at a Marman ring clamp on either side of the structure. The Marman ring on the orbiter and lander side both have a V-shaped groove which are held together with a circular clamp to maintain axial pressure. The clamp is held together by a pyrotechnic bolt that releases the clamp pressure upon its destruction. Once the clamp is released, several springs push the lander away from the orbiter bus until it has achieved a large enough separation distance to begin its deorbit burn. The primary maneuvering thrusters are located in a ring configuration about the center of mass of SAMUS when both landers are in their stowed configuration. Notably, these thrusters are not oriented along the long axis of the spacecraft due to the configuration of the landers. This design choice was motivated by the desire to minimize the mass of auxiliary structures around the landers' aeroshells. It should be noted that these thrusters will no longer act through the center of mass after one lander has been deployed, but while unconventional, the thruster placement does not impede the mission since the primary thrusters will not be utilized between the two lander deployment events.

The primary purposes of the lander structure are to protect the science instruments during the entry, descent, and landing procedure and to provide a platform for the components necessary to operate the instruments. The landers feature a tetrahedral structural design with deployable "petals." Since the SAMUS mission features two landers, minimizing mass wherever possible is of particular importance. For this reason, the petals are comprised of a lightweight composite honeycomb structure. Titanium fittings are bonded onto the lander structure along the contact points of the tetrahedron. These fittings are bolted together with pyrotechnic separation nuts that release after the landing sequence. Before the pyrotechnic bolts have been released, a set of winches mounted to the primary petal pull the deflated airbags back toward the lander. The accelerometer integrated into the lander's CPU is used to determine the orientation of the lander. The lander uses this information to determine which petal to open first to ensure that the lander deploys in the upright position. Each petal of the lander is outfitted with deployment latches that the robotic arm can grip. The robotic arm is used to push the lander into the upright position from the inside.

Orbital Dynamics

Determining an Interplanetary Transfer Orbit is fundamentally similar to the concept of leading the shot when throwing an object at a moving target. If we know where the spacecraft is at two points in time, at Earth at time of departure and at Mars at time of arrival, and the time of flight between those two points at time, we can solve for a singular elliptical orbit. This process, named for 18th century Mathematician Johann Lambert, who initially posed the problem [9]. An algorithm written by R.H. Gooding [8] based on Lambert's Problem can numerically solve the boundary value problem for the Fundamental Two-Body Equation (Equation 5). The results of the algorithm are the respective initial and final velocity vectors corresponding to departure and arrival, which thus can provide an appropriate estimate of the required v_∞ value leaving Earth's sphere of influence. Associated with v_∞ is characteristic energy (Equation 6), which describes the excess specific orbital energy leaving the sphere of influence. This value is directly related to the performance capabilities of standard launch services. Thus, this value should be minimized to deliver the maximum possible system mass.

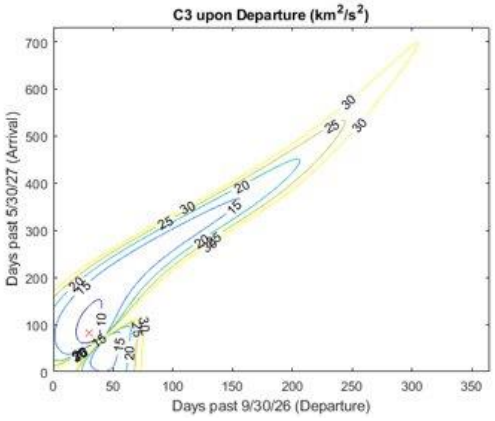

Figure 26 Transfer Orbit Optimization Porkchop Plot

$$\ddot{\vec{r}} = -\mu_{Sun} * \frac{\hat{r}}{r^2} \tag{5}$$

$$C_3 = v_\infty^2 \tag{6}$$

By repeating this process for every viable combination of departure and arrival dates and creating a pork chop plot (Figure 26) of values of C_3 associated with each transfer window, we can select the window which yields the lowest characteristic energy. Figure 27 show the Interplanetary Trajectory for the selected window.

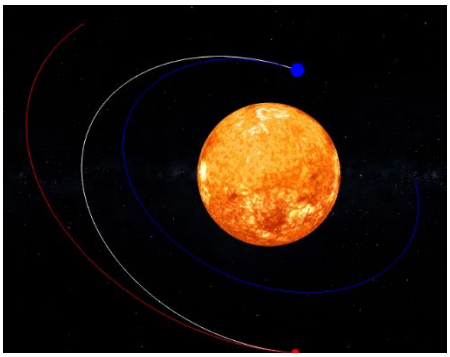

Figure 27 Interplanetary Transfer Orbit for 10/30/26-08/21/27

Aerobraking Simulation

The aerobraking process was modeled in Systems Toolkit using the 2010 Mars Global Reference Atmospheric Model [10], which has been used in previous missions, including Odyssey, Mars Reconnaissance Orbiter, Pathfinder, and the Mars Polar Lander. For additional fidelity, third body effects from Phobos and Deimos were considered as well. For simplification, a standard drag coefficient of 0.45 and a reference area of 17.5 m^2 way used based off the final orbiter configuration Figure 28 shows how the orbit precesses over the 19-week maneuver, along with a simplified

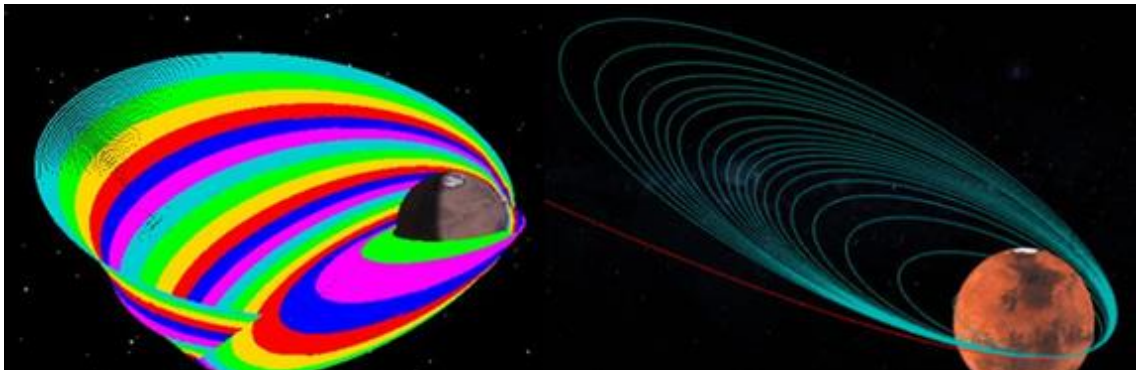

Figure 28 Aerobraking Maneuver computed in Systems Toolkit (left), Simplified Aerobraking Visualization (right). One color band/ellipse is one week.

version. The final ascending node and argument of periapsis do not matter, as the final ground track will eventually phase into position. Additionally, the orbit inclination does not deviate from 20 degrees for the entire process.

When selecting the dimensions of the initial elliptical orbit, there was a tradeoff between aerobraking viability and required ΔV for insertion from a hyperbolic arrival and recircularization at the final orbit altitude (Equation 7). describes the ΔV required for insertion, with V_{P1} and V_{P2} being the spacecraft velocities before and after insertion. Equation 8 describes the ΔV required for circularization after Aerobraking, with V_a being the apoapsis velocity prior to the maneuver and V_c being the final circular velocity. The initially selected orbit of 33,300x3550 km would have yielded a ΔV of 0.8916 km/s, but the simulation suggests that the aerodynamic drag at periapsis would not have been sufficient to lower the apoapsis. An elliptical orbit of 27,000x3480 km was selected, requiring only an additional 0.0181 m/s of ΔV for the two maneuvers.

$$V_{P1} = \sqrt{2 * \left(\frac{v_\infty^2}{2} + \frac{\mu}{r_P}\right)} \qquad V_{P2} = \sqrt{\mu * \left(\frac{2}{r_p} - \frac{1}{a}\right)} \qquad \Delta V = |V_{P2} - V_{P1}| \tag{7}$$

$$V_a = \sqrt{\mu * \left(\frac{2}{r_a} - \frac{1}{a}\right)} \qquad V_c = \sqrt{\frac{\mu}{r_c}} \qquad \Delta V = |V_c - V_a| \tag{8}$$

Ground Track Phasing

The two landing zones were selected for their flat terrain, low absolute latitude, and vicinity to the Valles Marineris. From this, the final orbit altitude of 110km was selected based upon a viable ground track, visualized in Figure 29.

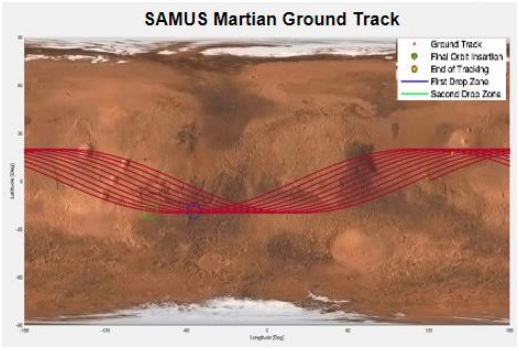

Figure 29 Ground Track at 3500km orbit

To pass over these points, the final orbit would have to have an inclination of 20 degrees. As previously described, SAMUS would arrive at this inclination based on the transfer orbit. Ground Track Phasing can be described by a westward drift over the course of one satellite orbital period, or one revolution times the ratio between the satellite orbit period and one Mars sidereal day. As expressed in Equation 9, from a desired westward drift, we can solve for the orbit radius, and thus altitude which would yield this phasing.

$$\Delta E = \omega_P * T_s = 2\pi * \frac{T_s}{T_P} \qquad T_s = 2\pi\sqrt{\frac{a^3}{\mu}} \qquad a = \sqrt[3]{\mu * \left(\frac{T_s}{2\pi}\right)^2} = \sqrt[3]{\mu * \left(\frac{\Delta E * T_P}{4\pi^2}\right)^2} \quad (9)$$

Deorbit Burn

The required ΔV to deorbit each of the landers is described by Equation 10, which resembles the first burn in a Hohmann transfer. This was selected, as it is the least required ΔV to transition between two circular orbits. Figure 30 shows this process, with the circular orbit exaggerated for visual purposes.

$$\Delta V = \sqrt{\frac{\mu}{r_1}} * \left(\sqrt{\frac{2r_2}{r_1+r_2}} - 1\right) \quad (10)$$

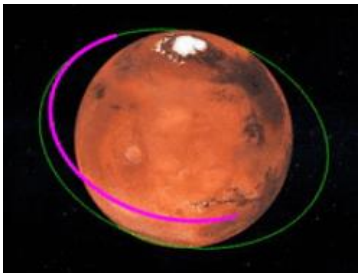

Figure 30 Lander Deorbit for Entry, Descent, and Landing

Mass Analysis

Mass analysis was performed by collecting information on historical Mars mission of similar budget and scope. A top-down approach was used to initially estimate the subsystem masses, based on our science payload mass, by comparing ratio of payload mass to lander mass, and bus payload (lander) mass to spacecraft mass. This analysis produced our level one and level two mass breakdown. For the level three mass breakdown, a bottom-up approach was used, individually adding the masses of known components to the budget. The discrepancy between level two and level three acts as an additional mass margin to prevent mass budget overshoot. This approach allows us to obtain the accuracy afforded by utilizing historical models, while simultaneously allowing for granularity in the level 3 budget without sacrificing margin. Table 6 shows the top-down mass level two mass budget while the bottom-up level three mass budgets are shown in their respective subsystem sections.

Table 6 Level 2 Mass Budget

	Level 2			Level 1
	CBE	Cont.	Allocated	
1.0 Payload				361.12
1.1 Landers x2	294.78	15%	339.12	
1.2 Probe Mounting Hardware	20.00	10%	22.00	
2.0 Spacecraft Bus Dry				2159.51
2.1 Propulsion	311.24	10%	342.36	
2.2 ADCS	143.65	10%	158.01	
2.3 Communications	167.59	10%	184.35	
2.4 CD&H	95.77	10%	105.34	
2.5 Power	502.77	10%	553.04	
2.6 Structure	598.53	10%	658.39	
2.7 Thermal Control	143.65	10%	158.01	
3.0 Spacecraft Dry Mass				2520.63
4.0 Consumables				0.00
5.0 Propellant				1351.60
6.0 Loaded Mass				3872.23
7.0 Kick Stage				0.00
8.0 Injected Mass				3872.23
9.0 Launch Vehicle Adapter				100.00
10.0 Boosted Mass				3972.23
11.0 Margin				1227.77
12.0 Total LV Capacity				5200.00

Management

Team Structure

There are nine team members assigned to the SAMUS mission. Each team member fulfills a predefined role based on their individual skills. The definitions for each role and the team member that will be fulfilling them are listed below.

- Principal Investigator (PI) – Dominic Hernandez: The PI shall have full responsibility for the scientific integrity of the mission and the assorted scheduling of executing the investigation within the committed cost and schedule.
- Deputy Principal Investigator (DPI) – George Frampton: The DPI shall fulfill the roles of the PI in the case of their absence.
- Project Manager (PM) – Dominic Hernandez: The project manager shall acquire a broad understanding of each subsystem, and be prepared to make decisions affecting cost, scheduling, and personnel assignment. The PM must also evaluate or be appraised of the risks associated with the execution of each system.
- Project Systems Engineer (PSE) – Dominic Hernandez: The project systems engineer shall have a comprehensive understanding of each system, from requirements to planning, configurations, interface and assessments. Design solution definitions and product verification processes are passed from this role to all subsystems.
- Trajectory and Entry Decent and Landing (EDL) Engineer – George Frampton: The trajectory and EDL engineer is primarily responsible for the calculation and visualization of astrodynamics parameters (launch windows, transfer orbit inclination changes, delta-vees for deorbiting maneuvers, etc). Additionally, development and assessment of strategies for entry, descent and landing also fall under this role.
- Thermal Protection System (TPS) & Thermal Control System (TCS) Engineer– Johy Ryu: Primarily responsible for determining optimal temperature profile for SAMUS craft electronics and possible extremes of temperatures faced during the mission, as well as procuring solutions to facilitate and mitigate these conditions, respectively.
- Propulsion - Ethan Hembree: Primarily responsible for researching propellant, P&ID and thruster solutions for SAMUS craft; including propellant types, tank volumes and thruster specifications.
- Power Systems - Garret Dreiband: Primarily responsible for drafting power budget for the SAMUS subsystems, as well as sizing calculations and considerations for power structures (power draw by instruments, solar array dimensions etc).
- Communications and Command & Data Handling (C&DH) – Gabi Nwachukwu: Primarily responsible for researching communications technology appropriate for the scope of the SAMUS mission and nature of data acquisition. Additionally, researching computing solutions and system configuration for data processing also falls under this role.
- CAD and Visualization - Anthony Limiero: Primarily responsible for producing previsualization and preliminary 3D models of the SAMUS craft in various configurations, working in tandem with other subsystem team leads to accommodate requirements.
- Guidance Navigation and Control (GNC) & Attitude Determination and Control System (ADCS) - Harrison Stewart: Primarily responsible for researching navigation and attitude control solutions for SAMUS craft. Partial responsibility overlap with propulsion team. Responsible for researching and determining the feasibility of the science investigation.

- Payload and Instrumentation - Thomas Baker: Primarily responsible for researching instrument suites to accomplish SAMUS science mission goals. Decisions made heavily influence CAD workflow, as spacecraft silhouette relies heavily on what data must be acquired.

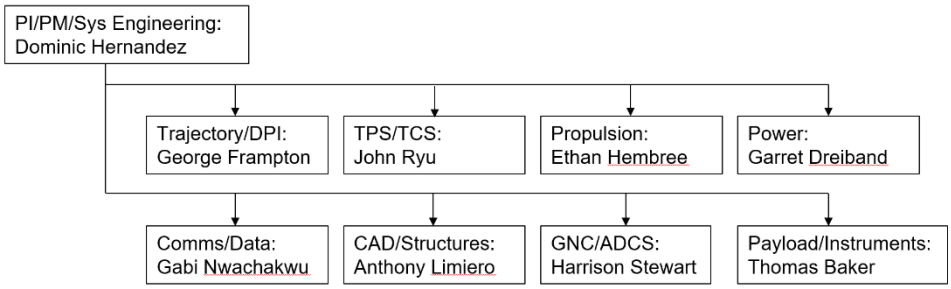

Figure 32 Team Organization Chart in WBS form

To comply with NPD 8020.7G and NID 8020.109A, a Planetary Safety Officer will be appointed. This officer will be responsible for prescribing standards, procedures, and guidelines to prevent the unwanted contamination of Mars during the operational phase of the proposed SAMUS mission. The Planetary Safety Officer will also be responsible for conducting routine reviews, inspections, and evaluations of ongoing operations and taking necessary action to ensure compliance with NASA's policies.

Mission categorization

The SAMUS project falls under the umbrella of MEPAG goals II and III, seeks to improve the resolution of science data collected by InSight and ExoMars TGO and has establish a projected life cycle cost (LCC) lies at $452.8M. The project team therefore proposes a Category 2 mission categorization.

Risks

We have identified five major risks to the development and implementation of the proposed SAMUS mission. Firstly, our target of interest, Valles Marineris, has geography that could prevent the deployment of our instruments and could potentially damage the lander upon landing (M1). While the geography in and directly around Valles Marineris is unforgiving, landing slightly farther away from the valley will mitigate this risk without greatly impacting the quality of the seismographic data collected. The prolonged aerobraking maneuver poses another risk to this mission (W2). The proximity of our spacecraft to Phobos and Deimos could cause unforeseen orbit perturbations and/or collisions. To mitigate this, continual orbital analysis of the spacecraft's orbit trajectory will be performed during mission implementation, and an excess propellant margin will be available for any unforeseen orbital correction maneuvers. A similar practice was employed on the Mars Reconnaissance Orbiter [16]. The arm being used to both deploy the petals of the lander that contain the solar panels, and the seismograph, is another potential failure point. The mechanical complexity of the arm, complexity of the maneuvers, and the consequences of failing to deploy the seismograph put this risk in the medium category (R3). This can, however, be mitigated by performing extensive testing on an analogous system on Earth before mission launch. Because the spacecraft bus is only utilizing a single four reaction wheel system, failure of two reaction wheels could render this specific system inoperable (R4). In this scenario, extra modeling can be done to allow the reaction wheel systems housed on the lander to perform the duties in place of the damaged system, with the existing ADCS thruster able to desaturate the wheels if necessary. The final identified risk to this mission is a launch window delay due to inclement weather (W5). A launch delay would result in a suboptimal Mars intercept velocity, possible exceeding what our propellant margins can account for. Mitigation for this risk is limited to monitoring weather activity and providing a propellant margin that can both, successfully capture the spacecraft in Mars orbit, without exceeding the launch vehicle payload for the given C3 during that launch window. Figure 31 depicts these risks, in this order, on the standard NASA risk matrix. Due to the short mission lifetime, medium to low cost of this mission, and alternative opportunities, the final risk class estimation according to NPR 8705.4 is Class C.

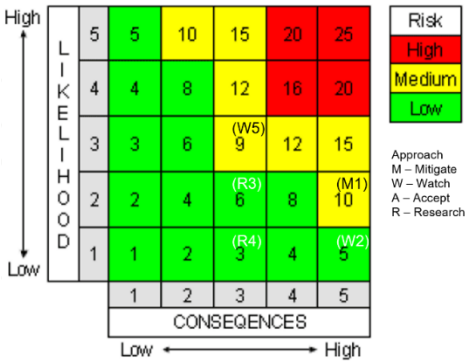

Figure 31 NASA risk matrix with current mission risks overlayed.

Cost and Schedule

To develop the schedule, the ideal launch date of October 30th, 2026 was used in conjunction with reference to a highly complex payload with new engineering. Though none of the instruments or science to be used on the bus or landers are emergent technology, there has yet to be a similar mission conducted using two landers implementing these instruments along with the robotics to deploy them. For these reasons, the highly complex and new references were most prudent for Phases A-D. As for Phase E, the operations lifetime was related directly to the lifetime of SEIS – about 2-3 years. The higher end of this range was decided as most accurate due to the relatively mild climate in which the landers will be placed as well as the ability for the lander petals to fold up and protect instrumentation during rough conditions. Utilizing all this information, a Gantt chart was developed (Figure 33) in order to dually track mission progress as well as maintain schedule requirements. The schedule assumes a start date of June 1st, 2022.

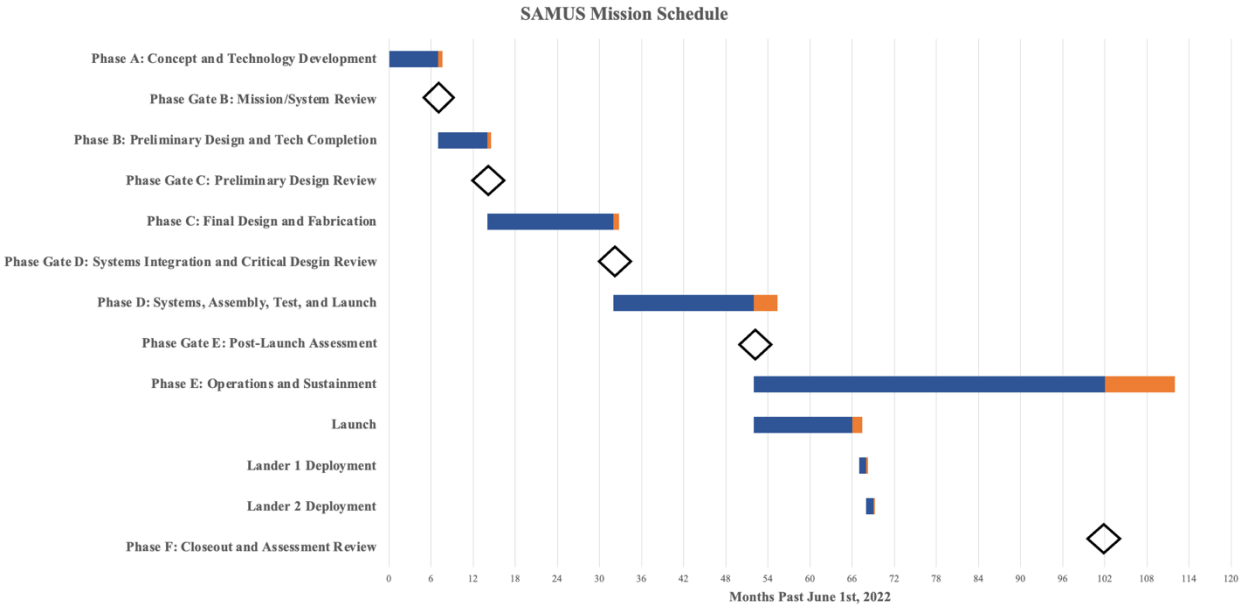

Figure 33 Mission Schedule Gantt Chart

Cost Estimation

The first step in determining the cost of the landers was determining the 2022 value of each item of the typical work-breakdown structure. Different methodologies were implemented as needed – the first costs calculated were those of the payload instruments. The cost of SEIS, REMS [7], and the aerobraking gears were able to be estimated via their previous research and development costs for other missions. Since these technologies have been previously developed, the cost of research – the bulk of the expense – was deducted leaving an estimation of what the price to simply develop replicas of these instruments.

As for the arm and camera, an analogous estimation approach was used as opposed to direct referencing. The reference used was the arm and camera developed by Motiv Space Systems for the 2020 Mars Perseverance Rover. Both, however, are significantly more powerful than what is necessary for the SAMUS landers. The Perseverance arm is capable of lifting 45 kg, while the lander arms are only required to lift the 29.5 kg SEIS. Additionally, the MastcamMars camera is extremely high definition and has features such as zooming and 3D video capture. For the landers, only a rudimentary telescoping camera is required to be able to evaluate drop zones for SEIS and taking inventory on the condition of the lander when necessary, so the cost estimate for them was significantly scaled down from the Perseverance cameras.

For all the subsystems of the spacecraft, including those which will be on the landers, a parametric cost estimation technique was utilized. The cost estimation relationship was pulled from *Space Mission Engineering: The*

New SMAD and provided a simple way to relate subsystem mass to production cost, and the calculations are shown in Figure 34 below [15].

From Table 11-7 from SME Text			
	Allocation	Dollars per Kg	Cost in FY2010$
2.1 Propulsion	342.3610667	$ 44,100.00	$ 15,098,123.04
2.2 ADCS	158.01	$ 165,900.00	$ 26,213,859.00
2.3 Communications	184.3482667	$ 82,500.00	$ 15,208,732.00
2.4 CD&H	105.3418667	$ 97,800.00	$ 10,302,434.56
2.5 Power	553.0448	$ 25,500.00	$ 14,102,642.40
2.6 Structure	658.3866667	$ 22,800.00	$ 15,011,216.00
2.7 Thermal Control	158.0128	$ 22,800.00	$ 3,602,691.84

Figure 34 Sub-system Mass Cost-Estimating Relationship

Finally, utilizing knowledge of the costs of the spacecraft and payload, historical wrap factors were implemented in determining the cost of over-head, level 1 necessities of the work-breakdown structure. Using wrap factors as an estimating tool has been the subject of several internal analyses at NASA. While it has not been proven as a universal solution, wrap factors are extremely useful at the lower end of class C and D missions – as management and MSA costs tend to scale evenly with hardware costs.

Inflation Considerations

While determining the estimated costs of each item, the year was additionally recorded in order to factor in inflation since the reference item was produced. For the purpose of model simplicity, a set inflation rate was chosen at 2.5% to represent yearly historical inflation as well as forward-facing inflation. 2.5% inflation is standard to be used for such a model, however macroeconomic factors have led to an unprecedented rise in inflation over the last year, raising the most recent CPI inflation estimation to 8.5% [19]. Knowing this, the inflation model used is quite optimistic at 2.5%, however the final budget was determined to withstand sustained future inflation of 4-5% if need be.

The first step in factoring inflation into the budget was to determine the net present value of each item in the budget dependent on the year that the prices were quoted from. Equation 11 as shown below was used:

$$NPV = P * (1 + i)^{(2022-Y)} \tag{11}$$

Where *NPV* is the net present 2022 value in USD, *P* is the price estimation USD, *Y* is the year the reference item was produced, and *i* is the inflation rate. Plugging all the values in, the present price for each item was determined and can be seen in Figure 35.

WBS Element	Cost Estimate	Year of Estimate	NPV Cost Estimate
1. Project Management	$ 28,000,000.00	2015	$ 36,846,089.82
2. Systems Engineering	$ 32,500,000.00	2015	$ 42,767,782.83
3. Safety and Mission Assurance	$ 13,000,000.00	2015	$ 17,107,113.13
4. Science/Technology	$ 10,744,017.63	2015	$ 14,138,394.24
5. Payload (Landers)			
5.1 SEIS x2	$ 30,000,000.00	2016	$ 37,959,570.55
5.2 REMS x2	$ 18,608,333.33	2009	$ 30,984,242.84
5.3 Arm x2	$ 15,000,000.00	2020	$ 16,224,000.00
5.4 Camera x2	$ 3,000,000.00	2020	$ 3,244,800.00
5.5 Lander Aerobraking x2	$ 4,000,000.00	1995	$ 11,533,474.30
6. Spacecraft			
6.1 Propulsion	$ 15,098,123.04	2010	$ 24,172,581.43
6.2 ADCS	$ 26,213,859.00	2010	$ 41,969,232.83
6.3 Communication	$ 15,208,732.00	2010	$ 24,349,669.94
6.4 CD&H	$ 10,302,434.56	2010	$ 16,494,529.66
6.5 Power	$ 14,102,642.40	2010	$ 22,578,784.85
6.6 Structure	$ 15,011,216.00	2010	$ 24,033,440.46
6.7 Thermal	$ 3,602,691.84	2010	$ 5,768,025.71
7. Mission Operation	$ 53,000,000.00	2015	$ 69,744,384.30
8. Launch Vehicle/Services	$ 3,792,006.22	2015	$ 4,990,021.50
9. Ground Systems	$ 16,432,026.97	2015	$ 21,623,426.48
10. Systems Integration and Testing	$ 12,500,000.00	2015	$ 16,449,147.24
11. Education and Public Outreach	$ 6,240,000.00	2020	$ 6,749,184.00

Figure 35 Budget Items Costs Normalized to 2022

These costs had to then be coupled with an approximate expenditure schedule. Given that SAMUS will take place over the course of 5+ years, the price estimation for each item has to be determined at the time when the money will actually be spent. Over a long time frame, inflation will inevitably alter the price of each item, and therefore must be accounted for. Each item's cost was split evenly over the years and phases which they will be necessary to get a rough estimation for a cost schedule. For example, project management will always be necessary, so its cost is split evenly over phases A-F. However, mission operations is only necessary once the mission has begun, so it's cost has been split evenly across phase E. Knowing the approximate year of each expenditure, a similar equation was implemented to determine the NPV needed to afford every item assuming it inflates.

$$NPV = P * (1 + i)^{(Y-2022)} \tag{12}$$

The symbols are all the same as the previous equation. Expanding costs over the course of the mission and factoring in inflation, the following overall budget shown in Figure 36 was determined:

	Phase A/B			Phase C		
WBS Element	FY 2022	FY 2023	Total Phase A/B NPV	FY 2023	FY 2024	Total Phase C NPV
1. Project Management	$ 3,698,133.46	$ 3,698,133.46	$ 7,488,720.25	$ 3,698,133.46	$ 3,698,133.46	$ 7,675,938.25
2. Systems Engineering	$ 6,438,714.50	$ 6,438,714.50	$ 13,038,396.86	$ 6,438,714.50	$ 6,438,714.50	$ 13,364,356.78
3. Safety and Mission Assurance	$ 1,716,990.53	$ 1,716,990.53	$ 3,476,905.83	$ 1,716,990.53	$ 1,716,990.53	$ 3,563,828.48
4. Science/Technology	$ 3,192,815.17	$ 3,192,815.17	$ 6,465,450.73	$ 3,192,815.17	$ 3,192,815.17	$ 6,627,087.00
5. Payload (Landers)						
5.1 SEIS x2				$ 8,697,700.64	$ 8,697,700.64	$ 18,053,164.88
5.2 REMS x2				$ 6,412,948.26	$ 6,412,948.26	$ 13,310,875.72
5.3 Arm x2				$ 3,939,843.75	$ 3,939,843.75	$ 8,177,638.18
5.4 Camera x2				$ 787,968.75	$ 787,968.75	$ 1,635,527.64
5.5 Lander Aerobraking x2				$ 1,947,800.02	$ 1,947,800.02	$ 4,042,902.41
6. Spacecraft						
6.1 Propulsion				$ 5,076,324.24	$ 5,076,324.24	$ 10,536,545.49
6.2 ADCS				$ 8,813,681.50	$ 8,813,681.50	$ 18,293,897.67
6.3 Communication				$ 5,113,513.42	$ 5,113,513.42	$ 10,613,736.30
6.4 CD&H				$ 3,463,907.28	$ 3,463,907.28	$ 7,189,772.54
6.5 Power				$ 4,741,621.54	$ 4,741,621.54	$ 9,841,828.21
6.6 Structure				$ 5,047,104.16	$ 5,047,104.16	$ 10,475,895.57
6.7 Thermal				$ 1,211,305.00	$ 1,211,305.00	$ 2,514,214.94
7. Mission Operation						
8. Launch Vehicle/Services						
9. Ground Systems						
10. Systems Integration and Testing				$ 3,714,642.98	$ 3,714,642.98	$ 7,710,205.84
11. Education and Public Outreach						
Reserves			$ 469,530,526.33			$ 315,903,110.44
PI Managed Mission Cost			$ 30,469,473.67			$ 184,096,889.56
Inflation:	1.025					

Phase D			Phase E				NPV$
FY 2025	FY 2026	Total Phase D NPV	FY 2027	FY 2028	FY 2029	Total Phase E NPV	Total
$ 3,698,133.46	$ 3,698,133.46	$ 8,064,532.63	$ 3,698,133.46	$ 3,698,133.46	$ 3,698,133.46	$ 12,868,718.15	$ 36,097,909.28
$ 6,438,714.50	$ 6,438,714.50	$ 14,040,927.34					$ 40,443,680.99
$ 1,716,990.53	$ 1,716,990.53	$ 3,744,247.29	$ 1,716,990.53	$ 1,716,990.53	$ 1,716,990.53	$ 5,974,762.00	$ 16,759,743.59
							$ 13,092,537.72
$ 8,697,700.64	$ 8,697,700.64	$ 18,967,106.36					$ 37,020,271.24
$ 6,412,948.26	$ 6,412,948.26	$ 13,984,738.81					$ 27,295,614.53
$ 3,939,843.75	$ 3,939,843.75	$ 8,591,631.12					$ 16,769,269.30
$ 787,968.75	$ 787,968.75	$ 1,718,326.22					$ 3,353,853.86
$ 1,947,800.02	$ 1,947,800.02	$ 4,247,574.35					$ 8,290,476.76
$ 5,076,324.24	$ 5,076,324.24	$ 11,069,958.11					$ 21,606,503.60
$ 8,813,681.50	$ 8,813,681.50	$ 19,220,026.24					$ 37,513,923.91
$ 5,113,513.42	$ 5,113,513.42	$ 11,151,056.70					$ 21,764,793.00
$ 3,463,907.28	$ 3,463,907.28	$ 7,553,754.77					$ 14,743,527.31
$ 4,741,621.54	$ 4,741,621.54	$ 10,340,070.76					$ 20,181,898.97
$ 5,047,104.16	$ 5,047,104.16	$ 11,006,237.78					$ 21,482,133.35
$ 1,211,305.00	$ 1,211,305.00	$ 2,641,497.07					$ 5,155,712.00
			$ 21,000,114.98	$ 21,000,114.98	$ 21,000,114.98	$ 73,075,935.19	$ 73,075,935.19
	$ 4,507,503.78	$ 4,975,440.77					$ 4,975,440.77
$ 3,906,503.27	$ 3,906,503.27	$ 8,518,925.42	$ 3,906,503.27	$ 3,906,503.27	$ 3,906,503.27	$ 13,593,800.80	$ 22,112,726.22
$ 3,714,642.98	$ 3,714,642.98	$ 8,100,535.01					$ 15,810,740.84
			$ 2,185,300.00	$ 2,185,300.00	$ 2,185,300.00	$ 7,604,379.37	$ 7,604,379.37
		$ 147,966,523.69					$ 34,848,928.18
		$ 352,033,476.31					$ 465,151,071.82

Figure 36 Overall Mission Budget

Note that the total cost shown below each phase is cumulative – so the $184 million figure under Phase C includes the $30 million incurred in Phases A-B and so on. The final PI-managed cost of the mission came out to $465,151,071.82, leaving the mission with $34,848,928.18 in reserves for inevitable surprise costs. There are a few notes of how the reserves are managed throughout the mission. Firstly, only $30,469,473.67 are projected to be spent prior to KDP-C, a mere 6.6% of the PI-managed mission cost. This ensures that a minimal loss will be incurred if the mission ends up being cancelled prior to development phase and is largely due to the use of technologies used in previous missions. In addition to low early-stage costs, the mission maintains $147,966,523.69 unencumbered costs through phases A-D – just above 29% of the total reserves. The PI will work closely with the Mission Operations team to ensure that maximal reserves are kept throughout Phase E, as Mission Operations are the large bulk of costs throughout this phase. Certain budget cuts may be necessary if too many extraneous costs are incurred throughout the development phase, however the presence of over $30 million in reserves upon closeout should provide more than enough to hedge against these problems.

References

[1] “11.0 Ground Data Systems & Mission Operations,” SOA of Small Spacecraft Technology, NASA, 2021, pp. 268–336.

[2] Buabthong, P., Ifkovits, Z. P., Kempler, P. A., Chen, Y., Nunez, P. D., Brunschwig, B. S., Papadantonakis, K. M., and Lewis, N. S., “Failure modes of protection layers produced by atomic layer deposition of amorphous tio2 on GaAs Anodes,” *Energy & Environmental Science*, vol. 13, 2020, pp. 4269–4279.

[3] Brustel, C., Flahaut, J., Hauber, E., Fueten, F., Quantin, C., Stesky, R., Davies, G. R., “Valles Marineris tectonic and volcanic history inferred from dikes in eastern Coprates Chasma,” Journal of Geophysical Research: Planets, 2017, pp 1353, https://doi.org/10.1002/2016JE005231

[4] Chin, D. K., “Frequency and Channel Assignments” NASA/DSN No. 810-005, 201, Rev. D.

[5] Cleveland, C. J., Ayres, R. U., and Iles, P., “Photovoltaic Conversion: Space Applications,” Encyclopedia of energy, Amsterdam: Elsevier Academic Press, 2005, pp. 25–33.

[6] “CNES to Build Seismometer for NASA’s Mars InSight Mission.” *SpaceNews*, 30 Nov. 1AD, spacenews.com/cnes-to-build-seismometer-for-nasas-mars-insight-mission/.

[7] Gomez-Elvira, Javier & Armiens, Carlos & Carrasco Blázquez, Isaías & Genzer, Maria & Gómez, Felipe & Haberle, Robert & Hamilton, Victoria & Harri, Ari-Matti & Kahanpää, Henrik & Kemppinen, Osku & Lepinette, Alain & Martin-Soler, Javier & Martín-Torres, F. J. & Martínez-Frías, Jesús & Mischna, Michael & Navarro Lopez, Sara & Newman, Claire & de Pablo, Miguel & Zorzano, María-Paz. (2014). Curiosity's rover environmental monitoring station: Overview of the first 100 sols. Journal of Geophysical Research: Planets. 119. 10.1002/2013JE004576.

[8] Gooding, R.H. “A procedure for the solution of Lambert's orbital boundary-value problem”. Celestial Mech Dyn Astr 48, 145–165 (1990). https://doi.org/10.1007/BF00049511

[9] James F. Jordon, “The Application of Lambert's Theorem to the Solution of Interplanetary Transfer Problems”, JPL TR 32-521, February 1964

[10] Justh, H. L. “Mars Global Reference Atmospheric Model 2010 Version: Users Guide” NASA/TM-2014-217499

[11] Knapmeyer-Endrun, B., Kawamura, T., “NASA’s InSight mission on Mars—first glimpses of the planet’s interior from seismology,” Nat Commun 11, 1451, 2020, pp. 1-3 https://doi.org/10.1038/s41467-020-15251-7

[12] Lognonné, P., Banerdt, W.B., Giardini, D. *et al.* SEIS: Insight’s Seismic Experiment for Internal Structure of Mars. *Space Sci Rev* **215,** 12 (2019). https://doi.org/10.1007/s11214-018-0574-6 [12] *Planetary Data System Archive*., “Seismic Experiment for Investigating the Subsurface (SEIS)- Software Interface Specification,” Sep. 2020.

[13] Planetary Data System Archive., “Seismic Experiment for Investigating the Subsurface (SEIS)- Software Interface Specification,” Sep. 2020.

Planetary Data System Archive., “Seismic Experiment for Investigating the Subsurface (SEIS)- Software Interface Specification,” Sep. 2020.

[14] Scot C.R. Rafkin, Robert M. Haberle, Timothy I. Michaels, “The Mars Regional Atmospheric Modeling System: Model Description and Selected Simulations,” Icarus, Vol. 151, Issue 2, 2001, pp. 228-229 https://doi.org/10.1006/icar.2001.6605.

[15] Shao, Anthony, et al. *Space Mission Engineering - the New SMAD. Workbook*. Hawthorne, Ca Microcosm Press, 2011.

[16] Stacia M. Long, Tung-Han You, C. Allen Halsell, Ramachand S. Bhat, Stuart W. Demcak, Eric J. Graat, Earl S. Higa, Dr. Dolan E. Highsmith, Neil A. Mottinger, Dr. Moriba K. Jah, “Mars Reconnaissance Orbiter Aerobraking Daily Operations and Collision Avoidance” Proceedings of the 20th International Symposium on Space Flight Dynamics, September 2007

[17] Stein, Seth, and Michael Wysession. “An Introduction to Seismology, Earthquakes, and Earth Structure,” Malden, MA: Blackwell Pub, 2003, pp. 169

[18] Sterz, S., Parmley, B., Caldwell, D., and Bennett, J., “Nickel-hydrogen (ni-H/sub 2/) Single Pressure Vessel (SPV) Battery Development Update,” *Thirteenth Annual Battery Conference on Applications and Advances. Proceedings of the Conference*, 1998, pp. 665–668.

[19] U.S. Bureau of Labor Statistics. “Consumer Price Index Summary.” *Bls.gov*, 10 Mar. 2022, www.bls.gov/news.release/cpi.nr0.htm